Optimising NMR Spectroscopy through Method and Software Development (?)

Jonathan Yong

University of Oxford

Contents

Abstract

I did stuff

Preface

Pulse sequence notation

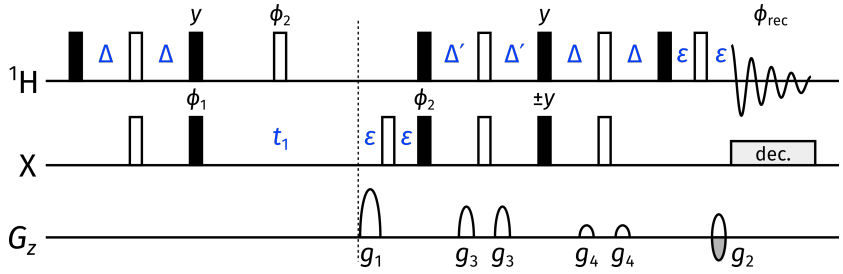

Figure 0.1: An example of a pulse sequence (the sensitivity-enhanced HSQC, see § 4.4.1), used here to illustrate the notation used in this thesis.

NMR pulse sequences in this thesis are depicted in a reasonably conventional manner: fig. 0.1 shows an example of this. The notation used is described here to avoid any ambiguity. Filled black rectangular bars indicate 90° pulses; empty bars indicate 180° pulses. Pulses with other flip angles are depicted using filled grey bars, typically with the Greek letter β above it representing the flip angle. Delays are variously represented by the letters Δ and τ; exact values of these will be given in the respective captions. Pulses without explicit phases are assumed to be applied along the rotating-frame $+x$-axis; phases of the form ϕ_i are typically cycled during the experiment and will be specified in the captions. Grey boxes labelled 'dec.' represent decoupling periods.

z-Gradient amplitudes are given as percentages of the maximum gradient amplitude, which is probe-dependent (see table 0.1). This maximum amplitude is unlikely to substantially affect the performance of any of the pulse sequences; consequently, in the text I quote gradient amplitudes only as percentages. Gradients which are inverted for echo–antiecho selection are depicted as a pair of positive and negative gradients (e.g. g_2 above). Note that whether the gradient is above or below the G_z line has no direct bearing on the sign of its amplitude (this may, in general, depend on the magnetogyric ratios of the nuclei being detected). ε is always used to denote the time required for a pulsed field gradient, plus the subsequent recovery delay.

In practice, the implementation of a pulse sequence may differ in tiny ways: for example delays

may be modified to accommodate finite pulse widths and other technicalities. Furthermore, shaped pulses may be used in place of hard pulses in order to optimise the pulse sequence, e.g. by allowing more efficient refocusing or excitation.

Software

All NMR data was processed using TopSpin 3 or 4. Quantum mechanical NMR simulations were done in Matlab R2021a or R2021b. This thesis is written using the LaTeX typesetting system: specifically, I used the LuaLaTeX engine.

Pulse sequences are drawn using the vector graphics programme Inkscape. Plots are generated using Python 3, using a number of packages (namely: `numpy`, `scipy`, `matplotlib`, `seaborn`, and `penguins`, the last of which was written by me, and described further in appendix A.1).

The underlying LaTeX code for this thesis, as well as all figures, can be accessed at TODO (likely GitHub).

Samples used

The caption of every figure showing experimental data includes a 'code' at the end, which indicates the spectrometer and sample used for the data. The available spectrometers and samples are enumerated in tables 0.1 and 0.2 and fig. 0.2. Therefore, for example, the code 7Z would represent data acquired on the 700 MHz spectrometer on the zolmitriptan sample.

Code	Internal name	Details
7	AV700	700 MHz ^{1}H resonance frequency 5 mm TCI ^{1}H/^{13}C/^{15}N inverse cryoprobe 53 G cm^{-1} maximum *z*-gradient amplitude AVANCE III console, TopSpin 3.6.2
6	AV600	600 MHz ^{1}H resonance frequency 5 mm Prodigy N_2 broadband cryoprobe (^{1}H/^{19}F outer coil) 66 G cm^{-1} maximum *z*-gradient amplitude AVANCE III console, TopSpin 3.6.2
4	AVB400	400 MHz ^{1}H resonance frequency 5 mm broadband (room-temperature) SmartProbe 50 G cm^{-1} maximum *z*-gradient amplitude AVANCE NEO console, TopSpin 4.0.8

Table 0.1: Spectrometers used in this thesis. A more complete description may be accessed via the links in the 'internal name' column.

Code	Compound	Solvent	Concentration
A	Andrographolide	DMSO-d_6	40 mM
B	(3-Fluorophenyl)boronic acid	DMSO-d_6	120 mM
C	Cyclosporin A	C_6D_6	50 mM
E	Ethanol	D_2O	1 M
F	Ferulic acid	DMSO-d_6	50 mM
G	Gramicidin S	DMSO-d_6	40 mM
H	Cholesterol	$CDCl_3$	50 mM
S	Sucrose	90% H_2O / 10% D_2O	22 mM
T	Ethyl ferulate	DMSO-d_6	200 mM
X	Brucine	$CDCl_3$	50 mM
Z	Zolmitriptan	DMSO-d_6	50 mM

Table 0.2: Samples used in this thesis. Note that concentrations are approximate and not necessarily constant, as samples were remade over time due to e.g. decomposition. However, it is reasonable to assume that the variation in concentration is below 10%. See fig. 0.2 for chemical structures.

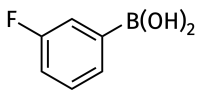

(3-fluorophenyl)boronic acid (**B**)

ethanol (**E**)

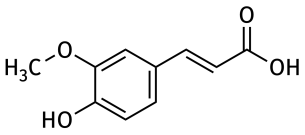

ferulic acid (**F**)

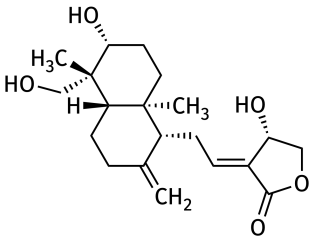

andrographolide (**A**)

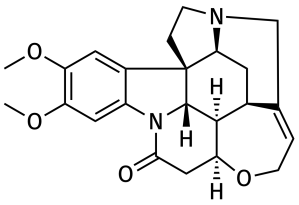

brucine (**X**)

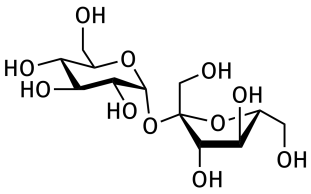

sucrose (**S**)

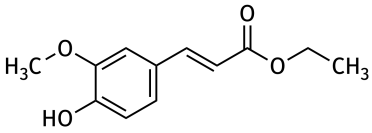

ethyl ferulate (**T**)

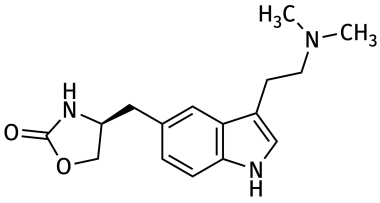

zolmitriptan (**Z**)

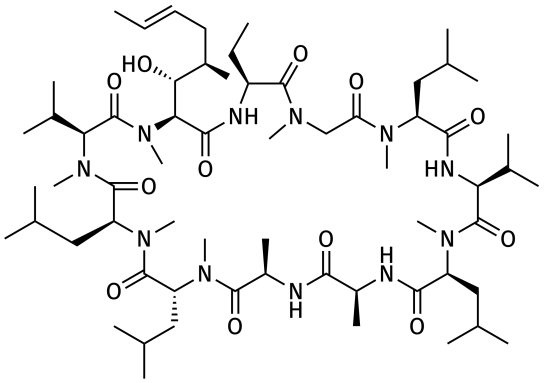

cyclosporin A (**C**)

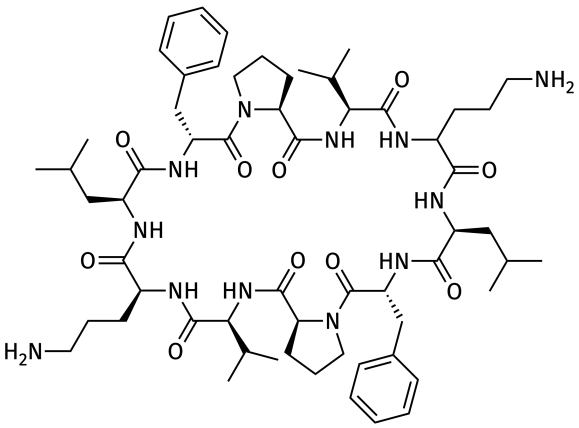

gramicidin S (**G**)

Figure 0.2: Chemical structures of samples used in this thesis. See table 0.2 for more information.

Acknowledgements

A quote goes here

By somebody

Thanks

Chapter 1

NMR theory

In the opening chapter of this thesis, I provide an overview of basic NMR theory, specifically, the dynamics of quantum systems containing one or more spin-½ particles. Starting from the Schrödinger equation, I progressively develop the formalisms used in the analysis and simulation of simple NMR experiments. The important product operator formalism, used throughout this thesis, is exemplified through a small number of 1D and 2D experiments.

Note that this is not designed to be an exhaustive account of magnetic resonance theory; the reader is directed to a suitable textbook on these topics.[1–5]

1.1 Quantum mechanics

The most fundamental equation in (non-relativistic) quantum mechanics, which governs the time evolution of a quantum state $|\Psi(t)\rangle$, is the time-dependent Schrödinger equation:

$$\frac{\partial|\Psi(t)\rangle}{\partial t} = -\frac{\mathrm{i}}{\hbar}H|\Psi(t)\rangle \tag{1.1}$$

For a Hamiltonian H which does not change during a period of time $t_1 \leq t \leq t_2$ (i.e. is *time-independent*), this can be integrated to yield an explicit solution:

$$|\Psi(t_2)\rangle = \exp\left[-\frac{\mathrm{i}H(t_2 - t_1)}{\hbar}\right]|\Psi(t_1)\rangle \tag{1.2}$$

In NMR, it is conventional to use units of angular frequencies instead of energies, for example by replacing $H/\hbar \rightarrow H$; this will henceforth be assumed. The term $\exp[-\mathrm{i}H(t_2 - t_1)]$ is called the *propagator* of the system and denoted $U(t_2, t_1)$; this is often further simplified to $U(\tau)$ where $\tau = t_2 - t_1$ is the duration of the evolution. For a Hamiltonian which varies with time but is piecewise constant, in that it can be broken up into several finite periods within which H is

time-independent, the time evolution of the state is simply given by successive application of propagators:

$$|\Psi(t_n)\rangle = U(t_n, t_{n-1}) \cdots U(t_2, t_1) U(t_1, t_0) |\Psi(t_0)\rangle \tag{1.3}$$

where $t_n > t_{n-1} > \cdots > t_0$. The case where H continuously varies with time is more complicated, but we will not need to consider it in this thesis.

In NMR spectroscopy, we manipulate the *spin angular momentum* of atomic nuclei in order to obtain information about chemical structure and dynamics. The present work is restricted to systems with spin quantum number $I = 1/2$. These are two-level systems, where the eigenstates of I_z (denoted as $|\alpha\rangle$ and $|\beta\rangle$ for $m_I = +1/2$ and $-1/2$ respectively) are used as a standard basis, called the *Zeeman basis*. The z-axis is conventionally chosen as the quantisation axis in textbook treatments of angular momentum (primarily for mathematical convenience), but in the context of NMR, it bears even more significance as we define the z-axis to be the axis along which the static magnetic field is aligned. Since the matrix elements of an operator O are given by $O_{mn} = \langle m|O|n\rangle$, we can work out the matrix representations of the angular momentum operators in the Zeeman basis:

$$I_x = \frac{1}{2}\begin{pmatrix} 0 & 1 \\ 1 & 0 \end{pmatrix}; \quad I_y = \frac{1}{2}\begin{pmatrix} 0 & -\mathrm{i} \\ \mathrm{i} & 0 \end{pmatrix}; \quad I_z = \frac{1}{2}\begin{pmatrix} 1 & 0 \\ 0 & -1 \end{pmatrix} \tag{1.4}$$

We also define the following linear combinations:

$$\begin{aligned} I_+ &= I_x + \mathrm{i}I_y = \begin{pmatrix} 0 & 1 \\ 0 & 0 \end{pmatrix}; \quad I_\alpha = \frac{1}{2}E + I_z = \begin{pmatrix} 1 & 0 \\ 0 & 0 \end{pmatrix} \\ I_- &= I_x - \mathrm{i}I_y = \begin{pmatrix} 0 & 0 \\ 1 & 0 \end{pmatrix}; \quad I_\beta = \frac{1}{2}E - I_z = \begin{pmatrix} 0 & 0 \\ 0 & 1 \end{pmatrix} \end{aligned} \tag{1.5}$$

where E is the 2×2 identity matrix. The *coherence order* of an operator, denoted p, is defined by the Zeeman basis states it connects, i.e. the nonzero elements in its matrix form when expressed in this basis: an operator $O = |m_2\rangle\langle m_1|$ would represent $(m_2 - m_1)$-order coherence, since $\langle m_2|O|m_1\rangle \neq 0$. Thus, in the above equations, $I_+ = |\alpha\rangle\langle\beta|$ represents a coherence order of $+1$; I_- a coherence order of -1; I_x and I_y are both a mixture of ± 1-coherence; and the remainder have coherence order 0.

States (and operators) for composite systems are formally defined as tensor products of single-spin states (and operators).[6] In matrix form, these can be expressed using the Kronecker product.[5]

Thus, for example, the operator $2I_xS_z$ could be represented as follows:*

$$2I_xS_z = 2 \cdot \frac{1}{2} \cdot \frac{1}{2}\left[\begin{pmatrix} 0 & 1 \\ 1 & 0 \end{pmatrix} \otimes \begin{pmatrix} 1 & 0 \\ 0 & -1 \end{pmatrix}\right] = \frac{1}{2}\begin{pmatrix} 0 & 0 & 1 & 0 \\ 0 & 0 & 0 & -1 \\ 1 & 0 & 0 & 0 \\ 0 & -1 & 0 & 0 \end{pmatrix} \tag{1.6}$$

The Hamiltonians H for nuclear spin interactions, which will be encountered frequently in this chapter, are formed from such operators.[3] In solution-state NMR, these interactions include:

$$H_{\text{cs}} = \sum_i \omega_{0,i} I_{iz} \qquad \text{(chemical shift)} \tag{1.7}$$

$$H_{\text{J}} = \sum_{i>j} 2\pi J_{ij} (\mathbf{I}_i \cdot \mathbf{I}_j) \qquad \text{(scalar coupling)} \tag{1.8}$$

$$H_{\text{pulse}} = \sum_i \omega_{i,x} I_{ix} + \sum_i \omega_{i,y} I_{iy} \qquad \text{(radiofrequency pulses)} \tag{1.9}$$

$$H_{\text{grad}} = \sum_i \gamma_i G z I_{iz} \qquad \text{(pulsed field gradients on } z\text{)} \tag{1.10}$$

Pulsed field gradients (henceforth shortened to *gradients*) can in principle be applied along any axis, not just z, but this is dependent on hardware: all the work in this thesis was done on z-gradient probes. In the above expressions:

- γ_i is the magnetogyric ratio of spin i;
- $\omega_{0,i}$ refers to the Larmor, or precession, frequency of spin i (usually on the order of MHz). The Larmor frequency is defined as

  $$\omega_{0,i} = -\gamma_i B_0, \tag{1.11}$$

  where B_0 is the strength of the external (static) magnetic field;
- J_{ij} is the scalar coupling constant between spins i and j (expressed in units of Hz);
- ω_x and ω_y are amplitudes of radiofrequency (RF) pulses along the x- and y-axes, which are in general time-dependent, and are related to the so-called B_1 by a factor of γ_i.
- G is the amplitude of the gradient, typically in units of G/cm; and
- z is the position of the spin along the z-axis, typically in units of cm.

*This representation is not unique; it is perfectly possible to reverse the order of the Kronecker product, and as long as this is consistently done, any physically measurable quantities calculated using this alternative will be the same.

Finally, note that in the *weak coupling* regime where

$$\omega_{0,i} - \omega_{0,j} \gg J_{ij}, \tag{1.12}$$

the scalar coupling Hamiltonian may be simplified (the *secular approximation**) to

$$H_{\mathrm{J,secular}} = \sum_{i>j} 2\pi J_{ij} I_{iz} I_{jz}. \tag{1.13}$$

This condition is always satisfied whenever spins i and j are different nuclides.

Throughout the course of an NMR experiment, RF pulses and gradients are turned on and off, and thus H_{pulse} and H_{grad} are time-dependent—although they will always satisfy the 'piecewise constant' criterion which allows us to use eq. (1.3). The 'free precession' (or simply 'free') Hamiltonian, H_{free}, refers to the Hamiltonian operative whenever no pulses or gradients are being applied:

$$H_{\mathrm{free}} = H_{\mathrm{cs}} + H_{\mathrm{J}}. \tag{1.14}$$

1.2 The rotating frame

The Hamiltonians described above refer to the 'laboratory frame' or the *Schrödinger picture*, where spins precess about the z-axis at their intrinsic frequencies and obey the equation of motion (1.1). However, this proves to often be unwieldy, in particular when analysing the effects of radiofrequency pulses. It is standard procedure to transform the frame of reference to a 'rotating frame', specifically, one which rotates about the z-axis at a defined rotation frequency ω_{rot} which is close to the Larmor frequencies ω_0.

The rotating frame can be formalised using the *interaction picture* of quantum mechanics,[6] which involves the separation of the Hamiltonian into two parts, with the first typically being completely time-independent:

$$H(t) = H_0 + H_1(t). \tag{1.15}$$

In this case, the static part H_0 simply corresponds to precession of the spins at a particular frequency:

$$H_0 = \sum_i \omega_{\mathrm{rot},i} I_{iz}. \tag{1.16}$$

(Generally, each instance of the same nuclide (e.g. ^{1}H or ^{13}C) will share the same ω_{rot}, so the

*This result comes from the use of time-independent nondegenerate perturbation theory: it is based on the assumption that the eigenstates $\{|n\rangle\}$ of the main Hamiltonian H_0 are unchanged by the perturbation V (since the first-order correction varies as $\sum_m V_{mn}/(\omega_m - \omega_n) \ll 1$), and only the first-order correction to the energies $E_n^{(1)} = \langle n|V|n\rangle$ is retained. In this context, H_0 and V are respectively H_{cs} and H_{J}. When the condition eq. (1.12) does not hold, the nondegenerate treatment fails; see e.g. Sakurai.[6]

subscript $\omega_{\text{rot},i}$ is useful only to distinguish different nuclear species.) This allows us to define H_1 as

$$\begin{aligned} H_1 &= H_\text{J} + H_\text{pulse} + H_\text{grad} + (H_\text{cs} - H_0) \\ &= H_\text{J} + H_\text{pulse} + H_\text{grad} + \sum_i \Omega_i I_{iz} \\ &= H_\text{J} + H_\text{pulse} + H_\text{grad} + H_\text{offset} \end{aligned} \tag{1.17}$$

where $\Omega_i = \omega_{0,i} - \omega_{\text{rot},i}$ is the *offset* of spin i. For reasons which will become clear later, the frequency ω_rot is chosen to be the centre of the spectral window for the given nuclide.

Having split up our Hamiltonian, we then define an *interaction-picture ket*:

$$|\Psi\rangle_I = \exp(\mathrm{i}H_0 t)\,|\Psi\rangle\,. \tag{1.18}$$

The time evolution of this ket is given by a transformation of the Schrödinger equation:

$$\begin{aligned} \frac{\partial |\Psi\rangle_I}{\partial t} &= \mathrm{i}H_0 \exp(\mathrm{i}H_0 t)\,|\Psi\rangle + \exp(\mathrm{i}H_0 t)\frac{\partial |\Psi\rangle}{\partial t} \\ &= \mathrm{i}H_0\,|\Psi\rangle_I + \exp(\mathrm{i}H_0 t)(-\mathrm{i}H|\Psi\rangle) \\ &= \mathrm{i}H_0\,|\Psi\rangle_I - \mathrm{i}\exp(\mathrm{i}H_0 t)(H_0 + H_1)\exp(-\mathrm{i}H_0 t)\,|\Psi\rangle_I \\ &= \mathrm{i}H_0\,|\Psi\rangle_I - \mathrm{i}H_0\,|\Psi\rangle_I - \mathrm{i}\exp(\mathrm{i}H_0 t)H_1\exp(-\mathrm{i}H_0 t)\,|\Psi\rangle_I \\ &= -\mathrm{i}\exp(\mathrm{i}H_0 t)H_1\exp(-\mathrm{i}H_0 t)\,|\Psi\rangle_I \\ &= -\mathrm{i}H_{1,I}|\Psi\rangle_I\,, \end{aligned} \tag{1.19}$$

where

$$H_{1,I} = \exp(\mathrm{i}H_0 t)H_1\exp(-\mathrm{i}H_0 t). \tag{1.20}$$

The underlying principle here is that the 'interesting' behaviour should be contained in H_1 (or rather $H_{1,I}$), and the interaction-picture states $|\Psi\rangle_I$ only evolve under this term. The effect of H_0 is not neglected, but rather it is 'absorbed' into the operators instead of the ket (eq. (1.20)).

We now turn our attention to how the various NMR Hamiltonians (eqs. (1.7) to (1.10)) are transformed in the interaction picture; that is to say, what the individual terms in the rhs of

$$\begin{aligned} H_{1,I} = \exp(\mathrm{i}H_0 t)H_\text{J}\exp(-\mathrm{i}H_0 t) + \exp(\mathrm{i}H_0 t)H_\text{pulse}\exp(-\mathrm{i}H_0 t) \\ + \exp(\mathrm{i}H_0 t)H_\text{grad}\exp(-\mathrm{i}H_0 t) + \exp(\mathrm{i}H_0 t)H_\text{offset}\exp(-\mathrm{i}H_0 t) \end{aligned} \tag{1.21}$$

are. We first note that H_0 (and hence $\exp(\pm\mathrm{i}H_0 t)$) is a function only of the I_{iz} operators; thus, any Hamiltonian which commutes with all I_{iz}'s will be untouched by this transformation. This is trivially true of H_offset and H_grad, which are themselves both functions of the I_{iz}'s. It can

also be shown that H_J (in the homonuclear case) and $H_{J,\text{secular}}$ (heteronuclear case) fully commute with H_0. So, for three out of the four terms in eq. (1.21) we simply have the result that $\exp(iH_0t)H\exp(-iH_0t) = H$. This allows us to immediately write down the free precession Hamiltonian in the interaction picture:

$$H_{\text{free},I} = H_{\text{offset}} + H_J. \tag{1.22}$$

The fourth term, which does not commute with H_0, is H_{pulse}. In the laboratory frame, *hard pulses* are applied as oscillating RF fields. Consider the case of a pulse acting on a single spin:

$$H_{\text{pulse,hard}} = \omega_1[\cos(\omega_{\text{rf}}t + \phi)I_x + \sin(\omega_{\text{rf}}t + \phi)I_y]. \tag{1.23}$$

Here, ω_1 represents the *amplitude* of the pulse, and ϕ the *phase*. This expression is similar to the expression in eq. (1.9), but here ω_1 and ϕ are both constants, with the time dependence explicitly specified using the *frequency* of the pulse, ω_{rf}. In the rotating frame, using that $H_0 = \omega_{\text{rot}}I_z$, we then have the following interaction Hamiltonian:

$$\begin{aligned} H_{\text{pulse,hard},I} = \omega_1 \big[&\exp(i\omega_{\text{rot}}tI_z)I_x\cos(\omega_{\text{rf}}t + \phi)\exp(-i\omega_{\text{rot}}tI_z) \\ &+ \exp(i\omega_{\text{rot}}tI_z)I_y\sin(\omega_{\text{rf}}t + \phi)\exp(-i\omega_{\text{rot}}tI_z)\big], \end{aligned} \tag{1.24}$$

and using the formulae

$$\exp(i\theta I_z)I_x\exp(-i\theta I_z) = I_x\cos\theta - I_y\sin\theta \tag{1.25}$$

$$\exp(i\theta I_z)I_y\exp(-i\theta I_z) = I_y\cos\theta + I_x\sin\theta \tag{1.26}$$

(see Appendix A.2 of Levitt[3] for a derivation), eq. (1.24) simplifies to

$$H_{\text{pulse,hard},I} = \omega_1\left[I_x\cos(\omega_{\text{rf}} - \omega_{\text{rot}} + \phi) + I_y\sin(\omega_{\text{rf}} - \omega_{\text{rot}} + \phi)\right]. \tag{1.27}$$

The frequency at which hard pulses are applied is termed the *transmitter frequency*, ω_{tx}. This is a parameter which can be controlled by the user, and is typically placed in the centre of the spectrum of the sample under study, in order to make the most use of its *bandwidth* (the region of frequencies over which the pulse is effective). For convenience, it is then typical to then choose the rotating-frame frequency to be exactly the same frequency: $\omega_{\text{rot}} = \omega_{\text{tx}}$ This allows us to simplify the rotating-frame Hamiltonian to

$$H_{\text{pulse,hard},I} = \omega_1(I_x\cos\phi + I_y\sin\phi), \tag{1.28}$$

which is time-*independent*. Occasionally, I will also use the Cartesian components:

$$(c_x, c_y) = (\omega_1\cos\phi, \omega_1\sin\phi), \tag{1.29}$$

instead of the amplitude and phase, to describe the pulse.

Consider now the application of this pulse to an isolated spin for which $\omega_0 = \omega_{\text{rot}}$ and thus has an offset $\Omega = 0$. We have that $H_{\text{offset}} = H_{\text{J}} = H_{\text{grad}} = 0$, and the only active Hamiltonian is that of the pulse, which causes *nutation* of the spin magnetisation vector around the axis of the pulse; in this case, the pulse (or the spin) is said to be *on-resonance*.* If a duration for the pulse τ_{p} is further specified, this also allows us to define a *flip angle* $\beta = \omega_1 \tau_{\text{p}}$. On the other hand, spins which are *off-resonance* ($\omega_0 - \omega_{\text{tx}} \neq 0$) evolve not only under the pulse Hamiltonian but also the offset; this leads to a different effective flip angle and axis of rotation. Off-resonance effects may be neglected when considering an idealised, infinitely hard pulse. However, this is of course not possible on a spectrometer, and in practice off-resonance effects are noticeable even for hard pulses as short as several microseconds.

In general, RF pulses are more complicated than the simple case of the hard pulse shown here. For example, they may be constructed such that even in the rotating frame there is still a time dependence in the amplitudes and/or the phases; these are often referred to as *shaped*, *amplitude-modulated*, or *frequency-modulated* pulses depending on the context. In principle, ω_1 and ϕ may both be continuous functions of time; however, for ease of construction and implementation, pulses are typically generated in a *piecewise* or discrete method using n points each of time δt, within which ω_1 and ϕ (or equivalently, c_x and c_y) are constant. The total length of the pulse is then simply $n(\delta t)$; δt is sometimes called the *timestep* of the pulse.

1.3 Density operators

NMR experiments are not executed on one single spin at a time: instead, the samples used typically contain $\sim 10^{20}$ spins. Furthermore, each of these spins may have its own wavefunction: it is generally impossible to force every spin to possess the same state. Since we are only interested in the *ensemble* behaviour such as expectation values, rather than the dynamics of each individual spin, we can use the *density operator* formalism instead of dealing with a composite wavefunction of many spins. The density operator, ρ, is defined (in the Schrödinger picture) as

$$\rho = \sum_j p_j \left|\psi_j\right\rangle \left\langle\psi_j\right| \tag{1.30}$$

*Strictly speaking, the rotating frame is just a mathematical formalism, so the resonance condition does not necessitate $\Omega = 0$ or $\omega_{\text{rf}} = \omega_{\text{rot}} = \omega_0$. We only need that $\omega_{\text{rf}} = \omega_0$, or in other words, that the pulse is applied at the frequency of the spin—which may or may not be the same as the rotating-frame frequency. Practically, such a situation may arise in (for example) the application of selective pulses to a specific spin which is not at the centre of the spectrum.

where p_j is the probability that a spin is in the state $|\psi_j\rangle$ (and the $|\psi_j\rangle$'s are assumed to form a complete set of states).* The use of ρ actually represents a loss of information, in that while eq. (1.30) gives us a straightforward recipe for constructing ρ from a given distribution of states $\{p_j, |\psi_j\rangle\}$, the reverse is not possible: given a known ρ, it is generally not possible to determine a unique distribution of states. This is not a problem, however, because ρ contains all the necessary information for calculation of expectation values, in that for any operator A,

$$\langle A\rangle = \sum_j \langle\psi_j|A\rho|\psi_j\rangle\,. \tag{1.31}$$

If A and ρ are expressed as matrices (through any choice of basis), then this is more easily expressed as the trace of the matrix product:

$$\langle A\rangle = \mathrm{Tr}(A\rho). \tag{1.32}$$

Other properties of the density operator are not discussed here, but can be found in virtually any textbook covering their use.[6–8]

The time evolution of a Schrödinger-picture density operator is governed by the Liouville–von Neumann equation, which can be derived from eq. (1.1):

$$\begin{aligned}\frac{\mathrm{d}\rho}{\mathrm{d}t} &= \sum_j p_j\left(\frac{\mathrm{d}\,|\psi_j\rangle}{\mathrm{d}t}\langle\psi_j| + |\psi_j\rangle\frac{\mathrm{d}\,\langle\psi_j|}{\mathrm{d}t}\right)\\ &= \sum_j p_j\left(-\mathrm{i}H|\psi_j\rangle\langle\psi_j| + |\psi_j\rangle\,\mathrm{i}\langle\psi_j|H\right)\\ &= -\mathrm{i}H\left(\sum_j p_j|\psi_j\rangle\langle\psi_j|\right) + \mathrm{i}\left(\sum_j p_j|\psi_j\rangle\langle\psi_j|\right)H\\ &= -\mathrm{i}[H,\rho].\end{aligned} \tag{1.33}$$

Note here that the weights p_j are time-independent, as the time evolution is contained entirely in the kets and bras.† For a time-independent H, this can be integrated to yield the solution:

$$\rho(t_2) = \exp(-\mathrm{i}H\tau)\rho(t_1)\exp(\mathrm{i}H\tau), \tag{1.34}$$

where $\tau = t_2 - t_1$.

In the interaction picture, the density operator is instead defined using interaction-picture states

*This probability is a *classical* probability: that is, it is purely statistical in nature and should not be confused with the probability amplitudes associated with quantum superposition (i.e. $|c_j|^2$ in a single-spin wavefunction $\sum_j c_j|j\rangle$).

†Strictly speaking, this only applies to a *closed* quantum system, which implies that effects such as relaxation are ignored (or at least, treated in only an empirical manner). The discussion of open quantum systems is beyond the scope of this work, but can be found elsewhere.[9,10]

$\{|\psi_i\rangle_I\}$:

$$\begin{aligned}\rho_I = \sum_j p_j |\psi_j\rangle_I \langle\psi_j|_I &= \sum_j p_j \exp(\mathrm{i}H_0 t)\,|\psi_j\rangle\,\langle\psi_j|\exp(-\mathrm{i}H_0 t) \\ &= \exp(\mathrm{i}H_0 t)\left(\sum_j p_j |\psi_j\rangle\langle\psi_j|\right)\exp(-\mathrm{i}H_0 t) \\ &= \exp(\mathrm{i}H_0 t)\rho\exp(-\mathrm{i}H_0 t) \end{aligned} \tag{1.35}$$

(note the similarity to eq. (1.20)). Using a very similar proof as in eq. (1.33), it can be shown that ρ_I obeys a modified Liouville–von Neumann equation:

$$\frac{\mathrm{d}\rho_I}{\mathrm{d}t} = -\mathrm{i}[H_{1,I}, \rho_I] \tag{1.36}$$

and analogously, for a time-independent $H_{1,I}$ we have that

$$\rho_I(t_2) = \exp(-\mathrm{i}H_{1,I}\tau)\rho_I(t_1)\exp(\mathrm{i}H_{1,I}\tau) = U\rho_I(t_1)U^\dagger, \tag{1.37}$$

where $U = \exp(-\mathrm{i}H_{1,I}\tau)$. Multiple propagators may be chained in a similar fashion to eq. (1.3). This result means that from a practical point of view, the effects of H_0 can be completely ignored when analysing or simulating NMR experiments using density operators.

Finally, a mention of the *equilibrium* or *thermal* density operator is in order. For a canonical ensemble, this is given by:

$$\rho_0 = \frac{\exp(-\beta\hbar H)}{\mathrm{Tr}[\exp(-\beta\hbar H)]} \tag{1.38}$$

where $\beta = 1/(k_\mathrm{B}T)$ and the Hamiltonian H is in units of angular momentum, as has been consistently used here. At equilibrium, no pulses or gradients are being applied, so the appropriate Hamiltonian is the free (Schrödinger-picture) Hamiltonian H_free (eq. (1.14)).* Consider the case of a single spin: we have that $H_\mathrm{J} = 0$, and hence $H_\mathrm{free} = H_\mathrm{cs} = \omega_0 I_z$. Thus,

$$\rho_0 = \frac{\exp(cI_z)}{\mathrm{Tr}[\exp(cI_z)]} \approx \frac{E + cI_z}{\mathrm{Tr}(E + cI_z)} = E + cI_z, \tag{1.39}$$

where $c = -\beta\hbar\omega_0 = -\hbar\omega_0/k_\mathrm{B}T$ and E is the identity matrix; the approximation $\exp(cI_z) \approx E + cI_z$ is justified here as c is typically very small ($\sim 10^{-5}$).

Throughout this thesis I consider only linear transformations of the form in eq. (1.37), which use

*It would be completely insensible to use the interaction-picture $H_{\mathrm{free},I}$, as its entire existence is merely a mathematical formalism. If that were not the case, it would imply that we can change the equilibrium state ρ_0 by simply *choosing* a different H_0 to factor out.

unitary propagators of the form $U = \exp(-\mathrm{i}Ht)$:

$$U\rho_0 U^\dagger = U(E + cI_z)U^\dagger = UEU^\dagger + c(UI_zU^\dagger) = E + c(UI_zU^\dagger) \tag{1.40}$$

When describing NMR experiments, it is typical to simply ignore both the E term as well as the proportionality factor c, and focus only on the transformation of the I_z term. Thus, one may define a 'simplified' equilibrium density operator:*

$$\rho_0' = I_z. \tag{1.41}$$

The E term is in fact truly inconsequential, as it cannot ever be transformed into detectable magnetisation. However, the constant c is still relevant: it is manifested in the magnitude of the NMR signal which is ultimately detected. It should be mentioned that ρ_0' is not a true density operator: for example, $\mathrm{Tr}(\rho_0') = 0$ and not 1 as is required for a density operator. Nonetheless, all the physically interesting dynamics of the system such as expectation values are fully contained within ρ_0' (at least up to the proportionality constant c).

1.4 Pulse sequences

It is impossible to provide a full overview of all, or even most, of the major NMR experiments in widespread use; the reader is directed to other books for this purpose.[2,4,5,13,14] I seek only to (somewhat briefly) explain the general structure of one- and two-dimensional Fourier transform experiments, and in particular, how the formalisms developed in previous sections can be used to analyse and simulate such experiments.

1.4.1 1D pulse–acquire

Consider the simplest NMR experiment, a 1D ^{1}H pulse–acquire spectrum (§ 1.4.1). This consists of a 90° pulse, immediately followed by detection; for convenience, we will first consider the pulse as being applied along the $+y$-axis, i.e. with a phase of $\phi = \pi/2$.

Figure 1.1: 1D ^{1}H pulse–acquire experiment.

*This is similar to the 'deviation' density operator[11,12] which measures how far a density operator deviates from the identity; but I have gone one step further in dropping the factor of c. Note that the alternative term 'reduced density operator' has a different meaning (it refers to the density operator of a subsystem, obtained by taking a partial trace over all other degrees of freedom).

To understand this, we begin with the thermal density operator $\rho_0' = I_z$ (eq. (1.41)) and assume that there is only one spin in the sample, and that the pulse is applied on-resonance. The corresponding Hamiltonian during the pulse is simply $\omega_1 I_y$ (eq. (1.28)). If the duration of the pulse is τ_p, then the density operator immediately following the pulse is given by:

$$\rho = \exp(-\mathrm{i}\omega_1 I_y \tau_\mathrm{p}) I_z \exp(\mathrm{i}\omega_1 I_y \tau_\mathrm{p}) = \cos(\omega_1 \tau_\mathrm{p}) I_z + \sin(\omega_1 \tau_\mathrm{p}) I_x. \tag{1.42}$$

In this case, to obtain a 90° pulse, τ_p is specifically calibrated to ensure that $\omega_1 \tau_\mathrm{p} = \pi/2$, which yields

$$\rho = I_x. \tag{1.43}$$

During the detection period, this term evolves under $H_\mathrm{free} = H_\mathrm{cs} = \omega_0 I_z$. (We use the Schrödinger-picture free Hamiltonian here because the measurement of the NMR signal takes place in the laboratory frame.) At a time t after detection has begun, the density operator is thus:

$$\rho(t) = \exp(-\mathrm{i}\omega_0 I_z t) I_x \exp(\mathrm{i}\omega_0 I_z t) = \cos(\omega_0 t) I_x + \sin(\omega_0 t) I_y. \tag{1.44}$$

The NMR signal derives from both x- and y-magnetisation (M_x and M_y), which are in turn proportional to I_x and I_y by a factor of γ. (If multiple spins are present, then each spin induces its own magnetisation: we would have that $M_x = \sum_i \gamma_i I_{ix}$, and likewise for M_y.) These are then combined to form a complex signal (this process is known as *quadrature detection*):

$$\begin{aligned} s(t) &= M_x(t) + \mathrm{i} M_y(t) && (1.45)\\ &\propto \langle I_x(t) \rangle + \mathrm{i} \langle I_y(t) \rangle \\ &= \mathrm{Tr}[I_x \rho(t)] + \mathrm{i}\,\mathrm{Tr}[I_y \rho(t)] \\ &\propto \cos(\omega_0 t) + \mathrm{i}\sin(\omega_0 t) \\ &= \exp(\mathrm{i}\omega_0 t). && (1.46) \end{aligned}$$

Before the signal is digitised, the NMR spectrometer mixes this with a *reference* RF field oscillating at the transmitter frequency ω_tx. This results in downconversion of the detected frequencies by ω_tx, such that the actual digitised signal oscillates at the offset frequency Ω rather than ω_0 (recall we have chosen $\omega_\mathrm{rot} = \omega_\mathrm{tx}$, so $\omega_0 - \omega_\mathrm{tx} = \omega_0 - \omega_\mathrm{rot} = \Omega$). Therefore, instead of eq. (1.46), the signal we really see is:

$$s(t) \propto \exp(\mathrm{i}\Omega t). \tag{1.47}$$

This result is the same as if we had pretended that during the detection period, ρ evolved under the *interaction-picture* free Hamiltonian $H_{\mathrm{free},I} = H_\mathrm{offset}$; we will henceforth adopt this simplification, even though it is not physically accurate.

In practice, relaxation causes this signal to decay with time; this is frequently modelled as an

exponential, in accordance with the Bloch equations:[15]

$$s(t) = \exp(\mathrm{i}\Omega t)\exp(-t/T_2), \tag{1.48}$$

where T_2 is the transverse relaxation time.* The NMR signal is thus often called a *free induction decay* (FID). Fourier transformation of the FID then yields a spectrum with absorption- and dispersion-mode lineshapes in the real and imaginary parts respectively (fig. 1.2):

$$S(\omega) = \mathscr{F}[s(t)] = \underbrace{\frac{k}{k^2 + (\omega - \Omega)^2}}_{A(\omega;\Omega)} + \mathrm{i}\underbrace{\frac{\Omega - \omega}{k^2 + (\omega - \Omega)^2}}_{D(\omega;\Omega)}, \tag{1.49}$$

where $k = 1/T_2$. The notation $A(\omega;\Omega)$ here means that the spectrum is a function of the frequency ω, but is parametrised by the peak offset Ω. Conventionally, only the real part of the spectrum is displayed, so it is desirable for the real part to contain the absorption-mode lineshape. This provides better resolution due to the narrower lineshape, and is also less affected by cancellation when multiple peaks overlap.

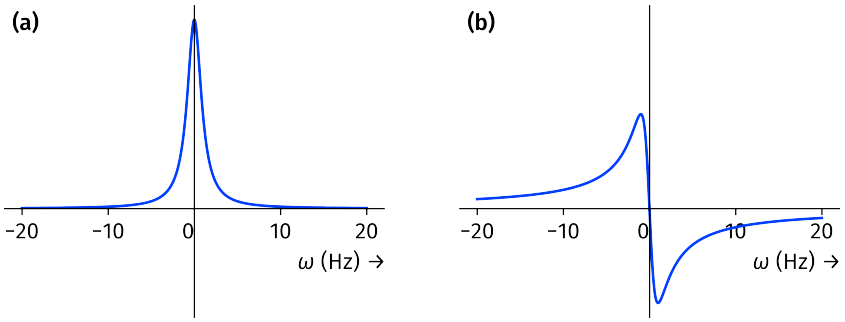

Figure 1.2: **(a)** Absorption-mode lineshape $A(\omega;\Omega = 0)$. **(b)** Dispersion-mode lineshape $D(\omega;\Omega = 0)$. Both lines have been plotted using $k = 1$ Hz.

Strictly speaking, the Lorentzian lineshapes above are only obtained when there is nonzero relaxation during the FID. For example, in the limit $k \to 0$, $A(\omega;\Omega)$ tends to a delta function $\delta(\omega = \Omega)$. However, for simplicity, in this thesis I will drop the relaxation term $\exp(-kt)$ unless absolutely necessary; I will simply pretend that a signal of the form $s(t) = \exp(\mathrm{i}\Omega t)$ is directly Fourier transformed to give $A(\omega;\Omega) + \mathrm{i}D(\omega;\Omega)$.

Consider now changing the initial pulse such that it is applied along the $+x$-axis instead ($\phi = 0$). Repeating the above analysis, we find that the resulting signal will have a phase shift:

$$s'(t) = -\mathrm{i}\exp(\mathrm{i}\Omega t) \tag{1.50}$$

$$\Rightarrow \quad S'(\omega) = \mathscr{F}[s'(t)] = D(\omega;\Omega) - \mathrm{i}A(\omega;\Omega). \tag{1.51}$$

*Transverse (and longitudinal) relaxation are sometimes called spin–spin (and spin–lattice) relaxation, although the continued usage of these terms has been criticised.[3,4,16]

If we were to take the real part of the spectrum here, then we would obtain the undesired dispersion-mode lineshape $D(\omega;\Omega)$. There are two ways of removing this phase shift. The first is to shift the *receiver phase* by ϕ_{rec}, which introduces an extra factor of $\exp(-\text{i}\phi_{\text{rec}})$ to the detected signal: we can thus choose $\phi_{\text{rec}} = 3\pi/2$ in order to cancel out the $-\text{i}$ term in $s'(t)$. Alternatively, the spectrum can be processed through *phase correction*, in which $S(\omega)$ is directly multiplied by a term $\exp(\text{i}\phi_{\text{corr}})$, where ϕ_{corr} is a linear function of the frequency ω:

$$\phi_{\text{corr}} = \phi_{\text{corr}}^{(0)} + \omega\phi_{\text{corr}}^{(1)}. \tag{1.52}$$

$\phi_{\text{corr}}^{(0)}$ and $\phi_{\text{corr}}^{(1)}$ are respectively termed the *zeroth-* and *first-order phase corrections*: in this idealised case, we can simply choose $(\phi_{\text{corr}}^{(0)}, \phi_{\text{corr}}^{(1)}) = (\pi/2, 0)$ to again remove the unwanted phase shift. More realistically, due to instrumental imperfections, both of these values will have to be nonzero in order to ensure that every peak in the spectrum has the correct phase, i.e. is displayed in absorption-mode.

An alternative framework for analysing pulse sequences is to use the ladder operators I_+ and I_- (eq. (1.5)). Using the original example with our initial pulse on $+y$, the density operator immediately after the pulse is:

$$\rho = I_x = \frac{1}{2}(I_+ + I_-), \tag{1.53}$$

and during detection this evolves as:

$$\rho(t) = \cos(\Omega t)I_x + \sin(\Omega t)I_y = \frac{1}{2}\left[\exp(-\text{i}\Omega t)I_+ + \exp(\text{i}\Omega t)I_-\right]. \tag{1.54}$$

(Notice that the $+1$-coherence I_+ actually evolves at the negative frequency $-\Omega$.) To obtain the same signal as previously done in eq. (1.46), we 'detect' the I_- term:

$$s(t) \propto \text{Tr}[I_-\rho(t)] \propto \exp(\text{i}\Omega t), \tag{1.55}$$

which leads to the common assertion that *only quantum coherences of order -1 are detectable.* It is true that coherences with orders $p = 0, \pm 2, \pm 3, \ldots$ can never be detected in an FID. However, it is worth pointing out that the 'uniqueness' of -1-coherence is merely a result of how the x- and y-magnetisation are combined to form the complex signal (eq. (1.45)). We do not *physically* detect I_-: we detect I_x and I_y, and combine them to form a complex signal which is mathematically equal to detecting I_-. If we had instead chosen to combine them in a different way, such as $s(t) = M_x(t) - \text{i}M_y(t)$, this would give us $s(t) \propto \exp(-\text{i}\Omega t)$—corresponding to 'detection' of $+1$-coherence—although this alternative does come with the drawback that frequencies must be reversed after Fourier transformation. In any case, we will stick to the established convention of detecting -1-coherence here.

To end this section, it should be pointed out that the complex signal is not obtained as an

infinitely-long, continuous function of time, as the treatment above implies. The complex-valued signal is digitised at an interval called the *dwell time*, τ_{dw}, and detection must be stopped after a finite period called the *acquisition time*, τ_{aq}. The Fourier transform being performed is actually a discrete Fourier transform (DFT), which yields a periodic function $S(\omega)$; its period (in Hz) is given by $1/\tau_{dw}$.* The NMR spectrum displayed to the user corresponds to one single period of $S(\omega)$, and thus the *spectral width* is also equal to $1/\tau_{dw}$.† In principle, the periodicity of the DFT means that signals which would ordinarily fall outside of the spectral width would appear at incorrect frequencies in the spectrum.[17] On modern instrumentation, this is no longer the case for direct detection; peaks outside of the spectral width are removed using digital filters. However, *folding* or *aliasing* of peaks in the indirect dimension(s) of multi-dimensional NMR spectra still occurs.

The DFT $S(\omega)$ is also a discrete function itself, and its resolution is given by $1/\tau_{aq}$. It is possible to extend the effective acquisition time (and thus improve spectral resolution) without actually acquiring more data: this can be done either by *forward linear prediction* of the signal, or by simply adding zeros onto the end of the signal (*zero-filling*).

1.4.2 INEPT and product operators

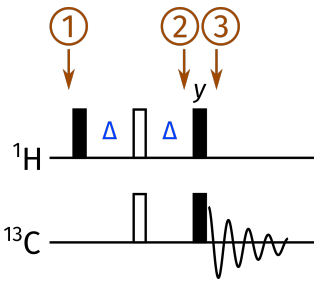

Figure 1.3: INEPT pulse sequence. The delay Δ is set to $1/(4 \cdot {}^1J_{CH})$.

Having tackled a simple single-spin case, we now move to the analysis of coupled spin systems and the development of the so-called 'product operator formalism'.[18] In particular, we look at the INEPT experiment,[19,20] in which magnetisation is transferred from a a nuclide with a high magnetogyric ratio to one with a low magnetogyric ratio through a scalar coupling: for example, from ^{1}H to ^{13}C using the one-bond coupling constant, $^1J_{CH}$ (fig. 1.3). Following tradition, the

*The periodicity property of the DFT is equivalent to the Nyquist theorem, which is usually formulated as follows: the sampling rate required to correctly digitise a signal containing frequencies in the range $[0, f_{max}]$ is $1/(2f_{max})$. In the main text, it appears as if we have dropped the factor of 2 in the denominator; but in truth this statement of the Nyquist theorem is applicable to *real-valued* signals, and here we have a *complex-valued* signal $s(t)$, which effectively doubles the range of correctly sampled frequencies.

†Frustratingly, the `DW` parameter in Bruker's TopSpin software is actually equal to $\tau_{dw}/2$. The reason is because this parameter corresponds to the interval between which *real* data is sampled, which is effectively twice as fast as complex-valued sampling.

two nuclei are respectively labelled I and S.* The Schrödinger-picture free Hamiltonian for a weakly coupled system (cf. eqs. (1.12) and (1.13)) is $H_{\text{free}} = \omega_{0,I} I_z + \omega_{0,S} S_z + 2\pi J_{IS} I_z S_z$. At the very beginning of the sequence (point ①), we formally have the equilibrium density operator

$$\rho_0 = \frac{\exp(-\beta\hbar H_{\text{free}})}{\text{Tr}[\exp(-\beta\hbar H_{\text{free}})]} \approx E - \beta\hbar(\omega_{0,I} I_z + \omega_{0,S} S_z + 2\pi J_{IS} I_z S_z), \tag{1.56}$$

using the same approximations as in eq. (1.39). The scalar coupling term can be safely neglected as $2\pi J_{IS}$ is several orders of magnitude smaller than the Larmor frequencies ω_0. After removing the physically irrelevant E term and factoring out a constant of $\beta\hbar B_0$, we end up with:

$$\rho_0' = \gamma_I I_z + \gamma_S S_z. \tag{1.57}$$

This represents equilibrium magnetisation (or *polarisation*) on both spins I and S, in proportion to their magnetogyric ratios. In general, an NMR experiment may manipulate—and ultimately detect—both of these terms. Since unitary evolution according to the Liouville–von Neumann equation is *linear*, in that $U(\rho_1 + \rho_2)U^\dagger = U\rho_1 U^\dagger + U\rho_2 U^\dagger$, we can treat these two terms separately: we focus first on the spin-I polarisation, $\rho_I = \gamma_I I_z$. The first 90°_x ^{1}H pulse tips this magnetisation into the transverse plane (ignoring off-resonance effects):

$$\rho_I \to \exp[-\text{i}(\pi/2)I_x]\gamma_I I_z \exp[\text{i}(\pi/2)I_x] = -\gamma_I I_y. \tag{1.58}$$

In principle, we could continue in this manner through repeated application of the 'sandwich' formulae (eqs. (1.25) and (1.26), as well as an analogous version for the $I_z S_z$ term). For example, in the Δ delay which follows, we have that

$$\begin{aligned} \rho_I &\to -\gamma_I \exp(-\text{i}H_{\text{free},I}\Delta) I_y \exp(\text{i}H_{\text{free},I}\Delta) \\ &= -\gamma_I \exp(-\text{i}H_{\text{J}}\Delta) \exp(-\text{i}H_{\text{offset}}\Delta) I_y \exp(\text{i}H_{\text{offset}}\Delta) \exp(\text{i}H_{\text{J}}\Delta) \\ &= \ldots \end{aligned} \tag{1.59}$$

When performing simulations of NMR experiments, such as those in later chapters, this is precisely what happens, with the slight difference that the Liouville–von Neumann equation (eq. (1.37)) is evaluated numerically rather than symbolically. Note that in going from the first to the second line, we can only 'split up' $H_{\text{free},I}$ into its constituent components H_{offset} and H_{J} because they commute.

When analysing pulse sequences by hand, however, it is far more convenient to use a set of heuristics which summarise the effects of various pulse sequence elements. For example, fig. 1.4

*This may seem insensible since I is the *sensitive* and S the *insensitive* nucleus, and indeed, in the original literature[19] the meanings of I and S were swapped. However, this usage has not been consistent,[21] and in modern usage the identification of I as the sensitive nucleus seems to have prevailed.

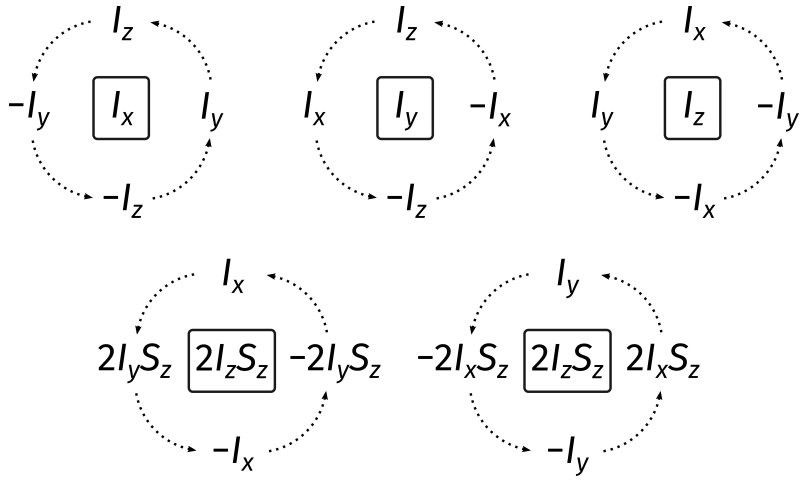

Figure 1.4: Simplified rules for the evolution of product operators under different common Hamiltonians (offset, weak/secular J-coupling, and pulses). These Hamiltonians often have the form ωM where M is some 'base operator', and are applied for a time τ. The boxed operators in the centre of each group refer to M; the initial state is then 'rotated' about this by an angle of $\omega\tau$ to obtain the final state, or more formally, it is transformed into itself times $\cos(\omega\tau)$, plus the next term in the cycle times $\sin(\omega\tau)$. For example, an 90°_x pulse has the 'base' operator I_x and the angle $\omega\tau = \pi/2$; thus, the initial state I_z would be rotated to $I_z\cos(\pi/2) - I_y\sin(\pi/2) = -I_y$.

summarises the evolution of a density operator under a single term of the Hamiltonian: as above, since $[H_{\text{offset}}, H_{\text{J}}] = 0$, we only need to consider one term at a time. More high-level rules may be devised as well: for example, during the Δ–$180^\circ_x(I)$, $180^\circ_x(S)$–Δ spin echo which comes next, the J_{IS} interaction in $H_{\text{free},I}$ is allowed to evolve for a period of 2Δ, but the offset term is *refocused* and can be ignored. (The sign inversion caused by the 180° pulses must also be included.) As per fig. 1.4, this transforms the $-I_y$ term to $-2I_xS_z$ at point ②: the Hamiltonian is $\pi J_{IS} 2I_zS_z$ for a total time of $2\Delta = 1/(2J_{IS})$, so the 'angle' rotated through is $\pi J_{IS}/(2J_{IS}) = \pi/2$. Immediately after this, the $90^\circ_y(I), 90^\circ_x(S)$ pair of pulses rotates this magnetisation to $-2I_zS_y$ (point ③). These transformations are often denoted with simpler notation:

$$\gamma_I I_z \xrightarrow{90^\circ_x(I)} -\gamma_I I_y \xrightarrow{\Delta-180^\circ_x(I),180^\circ_x(S)-\Delta} -2\gamma_I I_x S_z \xrightarrow{90^\circ_y(I),90^\circ_x(S)} -2\gamma_I I_z S_y \tag{1.60}$$

During the detection period, the term $-2\gamma_I I_z S_y$ evolves as

$$\begin{aligned} -2\gamma_I I_z S_y \xrightarrow{H_{\text{free},I}} &-2\gamma_I I_z S_y \cos(\Omega_S t)\cos(\pi J t) + \gamma_I S_x \cos(\Omega_S t)\sin(\pi J t) \\ &- 2\gamma_I I_z S_x \sin(\Omega_S t)\cos(\pi J t) + \gamma_I S_y \sin(\Omega_S t)\sin(\pi J t), \end{aligned} \tag{1.61}$$

from which we extract the complex signal

$$s_I(t) = \langle S_x(t)\rangle + \mathrm{i}\langle S_y(t)\rangle = \frac{\gamma_I}{2\mathrm{i}}\big\{\exp[\mathrm{i}(\Omega_S + \pi J_{IS})t] - \exp[\mathrm{i}(\Omega_S - \pi J_{IS})t]\big\}. \tag{1.62}$$

After Fourier transformation, the resulting spectrum has two peaks with opposite phase and have the frequencies $\Omega_S \pm \pi J_{IS}$; because of the factor of $1/(2\mathrm{i})$, the real part of the spectrum will contain dispersion-mode signals (fig. 1.5a). If desired, zeroth-order phase correction can be performed here, yielding instead a pair of absorption-mode signals still with opposite phases (fig. 1.5b). In either case, this is termed an *antiphase* doublet; the product operators which give rise to it ($2I_zS_x$ and $2I_zS_y$) are said to be antiphase with respect to spin I. Importantly, the amplitude of the signal scales as γ_I rather than γ_S; since $\gamma_I > \gamma_S$, this represents a sensitivity enhancement compared to the direct excitation of S-magnetisation.

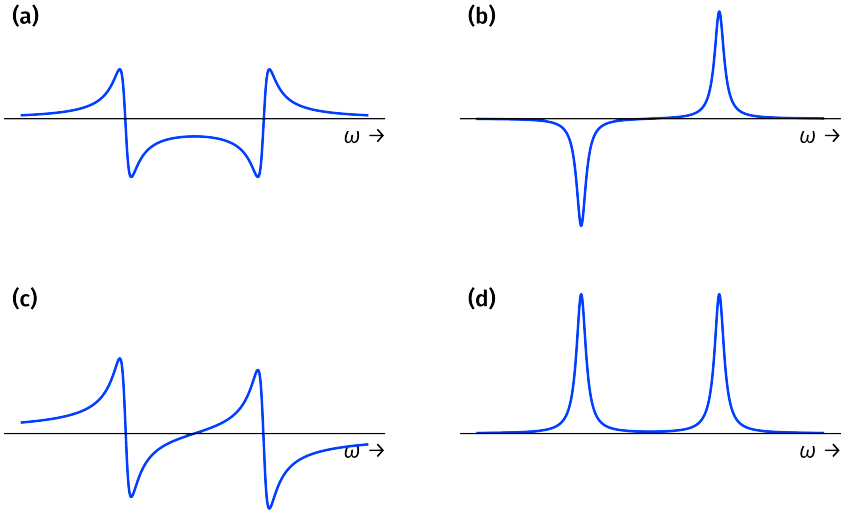

Figure 1.5: Peak shapes of a doublet. In all cases, the separation between the two peaks is $2\pi J_{IS}$. **(a)** Antiphase, dispersion-mode. **(b)** Antiphase, absorption-mode. **(c)** In-phase, dispersion-mode. **(d)** In-phase, absorption-mode.

Of course, this is only half of the picture; we have not considered what happens to the other part of the magnetisation, namely $\rho_S = \gamma_S S_z$. Clearly, this is unaffected by the initial $90^\circ_x(I)$ pulse and the first Δ delay. The $180^\circ_x(S)$ pulse inverts it, and the final $90^\circ_x(S)$ pulse in fact transforms it into observable S-magnetisation:

$$\gamma_S S_z \xrightarrow{90^\circ_x(I)-\Delta} \gamma_S S_z \xrightarrow{180^\circ_x(I),180^\circ_x(S)-\Delta} -\gamma_S S_z \xrightarrow{90^\circ_y(I),90^\circ_x(S)} \gamma_S S_y \tag{1.63}$$

This term produces *in-phase* spin-S magnetisation during the detection period (where the two components of the doublet have the same phase):

$$s_S(t) = \frac{\mathrm{i}\gamma_S}{2}\{\exp[\mathrm{i}(\Omega_S + \pi J_{IS})t] + \exp[\mathrm{i}(\Omega_S - \pi J_{IS})t]\}, \tag{1.64}$$

Because of the factor of i, the real part of the spectrum will contain a dispersion-mode doublet (fig. 1.5c). The signal actually measured by the spectrometer is $s(t) = s_I(t) + s_S(t)$; and the spectrum is a weighted sum of in-phase and antiphase magnetisation. This leads to potentially unwanted phase distortions in the spectrum, which one would prefer to suppress.

This can be accomplished through the technique of *phase cycling*, where pulse and receiver phases are changed in concert and the resulting FIDs summed in order to select for a particular signal. In this case, the INEPT experiment is performed twice, once with the phases as given in fig. 1.3, and once where the initial $90^\circ_x(I)$ pulse is replaced with a $90^\circ_{-x}(I)$ pulse. The first of these gives us the same signals as above. However, inverting the initial I pulse leads to s_I acquiring a minus sign, because the initial I_z term is rotated to I_y instead of $-I_y$. On the other hand, the signal component s_S is unaffected by this pulse and thus does not experience a change of sign. The two FIDs we record are thus as follows:

$$s_1(t) = s_I(t) + s_S(t) \tag{1.65}$$

$$s_2(t) = -s_I(t) + s_S(t) \tag{1.66}$$

Simply taking the difference of these two FIDs yields a signal where the desired s_I has been accumulated and s_S has been cancelled out. In practice, instead of subtracting the two signals, it is typical to shift the receiver phase ϕ_{rec} by 180° in the second experiment: this introduces a phase shift of $\exp(-\mathrm{i}\pi) = -1$ to the signal, and the two signals can now be *added* together instead of subtracted to cancel out s_S. Since both ϕ_1 and ϕ_{rec} are 0 on the first experiment and π on the second experiment, we can express this as $\phi_x = \phi_{\text{rec}} = (0, \pi)$. This is more commonly denoted as $\phi_1 = \phi_{\text{rec}} = (x, -x)$, because the phases $(0, \pi)$ correspond to the $+x$- and $-x$-axes respectively.

The 'simplified' analysis of pulse sequences shown in eqs. (1.60) and (1.63) is often called '*product operator*' analysis,[18] because the underlying two-spin operators are products of single-spin Cartesian operators. Although this is often touted as being 'simpler' than full density operator calculations, it is really just a shorthand which masks the quantum mechanical theory developed in this chapter:

$$\underbrace{I_z \xrightarrow{90^\circ_x(I)} -I_y}_{\textit{product operator}} \quad \Longleftrightarrow \quad \underbrace{\exp(-\mathrm{i}I_x\pi/2) I_z \exp(\mathrm{i}I_x\pi/2) = -I_y}_{\textit{density operator}} \tag{1.67}$$

Since the operators $\{E, I_x, I_y, I_z\}$ form a complete basis for a single-spin system, their products (i.e. product operators) likewise form a complete basis for multiple-spin systems, and so *any* density matrix for a multiple-spin system may be expressed as a linear combination of product operators. Strictly speaking, the use of product operators therefore does not actually sacrifice any power in and of itself. However, the heuristics such as those in fig. 1.4 *are* limiting, in that the evolution under some Hamiltonians—for example, strong coupling $\mathbf{I} \cdot \mathbf{S}$, or pulses for off-resonance spins where H is a sum of I_x and I_z—cannot be neatly captured in such a pictorial form.

1.4.3 2D NMR: general principles

Much of this thesis is concerned with two-dimensional (2D) NMR experiments. Before considering an explicit example of a 2D experiment, we will first describe some general principles. 2D experiments contain one *indirect* and one *direct* time dimension, traditionally labelled t_1 and t_2 respectively. The t_1 period is a variable period which starts at 0* and is incremented by a constant amount $\delta(t_1)$ on every iteration of the sequence. For each value of t_1 (or each t_1 *increment*) one complex signal $s'(t_2)$ is obtained. Putting this all together, the raw data is thus of the form $s(t_1, t_2)$, which can be viewed as a 2D data matrix. Fourier transformation in both dimensions leads to a spectrum $S(\omega_1, \omega_2)$. In experimental contexts, the frequency dimensions are often referred to as F_1 and F_2, but in this chapter I stick to the more mathematically consistent ω.

2D experiments generally comprise four components: *preparation*, *evolution*, *mixing*, and *detection*. The relevant product operators broadly follow this pattern:

$$\rho_0' \xrightarrow{\textit{preparation}} P \xrightarrow{\textit{evolution}} P\cos(\Omega_P t_1) + P' \sin(\Omega_P t_1) \xrightarrow{\textit{mixing}} Q\cos(\Omega_P t_1) + \cdots \quad (1.68)$$

Here, P is some operator which, during the t_1 period, evolves into P' at a frequency of Ω_P (as per fig. 1.4). This leads to two terms which are *amplitude-modulated* in t_1. The mixing process simply transforms the operator P to Q; for now, we will assume that the sine-modulated term P' is turned into unobservable magnetisation.

During the detection period, the x- and y-magnetisation generated by the term Q is recorded. As discussed in § 1.4.1, Q must therefore be (or at least contain) -1-quantum coherence on some spin, and thus evolves at the offset of that spin, Ω_Q. The complex signal $s(t_1, t_2)$ is therefore of the form $\cos(\Omega_P t_1)\exp(\mathrm{i}\Omega_Q t_2)$. Note that, since the term P is not directly detected, it can have *any* coherence order.

We can equivalently express this signal as a sum of complex exponentials, which is easier to Fourier transform:

$$s(t_1, t_2) = \cos(\Omega_P t_1)\exp(\mathrm{i}\Omega_Q t_2) = \frac{1}{2}\big[\exp(\mathrm{i}\Omega_P t_1)\exp(\mathrm{i}\Omega_Q t_2) + \exp(-\mathrm{i}\Omega_P t_1)\exp(\mathrm{i}\Omega_Q t_2)\big] \quad (1.69)$$

Fourier transformation of the first term reveals a peak centred at $(\omega_1, \omega_2) = (\Omega_P, \Omega_Q)$:

$$\begin{aligned}\mathscr{F}[\exp(\mathrm{i}\Omega_P t_1)\exp(\mathrm{i}\Omega_Q t_2)] &= [A_1(\Omega_P) + \mathrm{i}D_1(\Omega_P)][A_2(\Omega_Q) + \mathrm{i}D_2(\Omega_Q)] \\ &= A_1(\Omega_P)A_2(\Omega_Q) - D_1(\Omega_P)D_2(\Omega_Q) \\ &\quad + \mathrm{i}[A_1(\Omega_P)D_2(\Omega_Q) + D_1(\Omega_P)A_2(\Omega_Q)], \end{aligned} \quad (1.70)$$

*Or *as close to 0 as possible*, considering that pulse elements during t_1—such as the $180^\circ(I)$ pulse in fig. 1.6—require finite amounts of time. In some cases, it is possible to arrange spin echoes around t_1 such that the t_1 evolution on the first increment is refocused.

where we have used the shorthand $A_i(\Omega)$ to denote what should properly be written as $A(\omega_i;\Omega)$. We should ideally like our 2D peaks to be absorption-mode in both dimensions, i.e. $S(\omega_1,\omega_2) = A_1(\Omega_P)A_2(\Omega_Q)$. Unfortunately, if we take the real part of this spectrum, we have an undesirable mixture of double absorption and double dispersion: this peak shape is called a *phase twist*.

This is not the only problem, however: if we perform the same Fourier transformation on the second term in eq. (1.69), we get *another* phase twist peak but this time centred at $(\omega_1,\omega_2) = (-\Omega_P,\Omega_Q)$. So, merely obtaining the complex signal $s(t) = \cos(\Omega_P t_1)\exp(\mathrm{i}\Omega_Q t_1)$ is clearly not good enough. Firstly, our spectra are not *pure phase* or *phase-sensitive*, in that the peaks are an inseparable mixture of absorptive and dispersive lineshapes. Secondly, we have lost *quadrature detection* in the indirect dimension, in that we cannot distinguish positive from negative offsets.

There are multiple different ways of solving these dual issues, which are extensively covered in NMR textbooks.[1–4,14] Among these are the States method,[22] the TPPI method,[23] and the echo–antiecho method. I will briefly cover the States and echo–antiecho methods; the TPPI method can be shown to be essentially mathematically equivalent to the States method.[24⋆]

In the States method, the cosine-modulated signal described above (and denoted $s_{\cos}(t_1,t_2)$ here) forms only one part of the signal. It is also necessary to acquire a *sine-modulated signal* of the form $s_{\sin}(t_1,t_2) = \sin(\Omega_P t_1)\exp(\Omega_Q t_2)$. Once we have these two datasets, we can perform a Fourier transform along ω_2 first to get two intermediate signals:

$$s'_{\cos}(t_1,\omega_2) = \cos(\Omega_P t_1)[A_2(\Omega_Q) + \mathrm{i}D_2(\Omega_Q)] \tag{1.71}$$

$$s'_{\sin}(t_1,\omega_2) = \sin(\Omega_P t_1)[A_2(\Omega_Q) + \mathrm{i}D_2(\Omega_Q)]. \tag{1.72}$$

(If desired, phase correction along the ω_2 dimension *must* be performed at this stage before moving on.) We then discard the imaginary parts of these signals and use their real parts to construct another complex signal:

$$s''(t_1,\omega_2) = \Re\{s'_{\cos}(t_1,\omega_2)\} + \mathrm{i}\Re\{s'_{\sin}(t_1,\omega_2)\} = \exp(\mathrm{i}\Omega_P t_1)A_2(\Omega_Q). \tag{1.73}$$

Fourier transformation along ω_1 yields

$$S(\omega_1,\omega_2) = [A_1(\Omega_P) + \mathrm{i}D_1(\Omega_P)]A_2(\Omega_Q), \tag{1.74}$$

which represents a peak only at the correct frequency (Ω_P,Ω_Q), and the real part of which is the

⋆There is a slight difference in that the TPPI method pushes *axial peaks*—artefacts arising at $\omega_1 = 0$—to the edge of the spectrum, whereas with the States method, these artefacts appear in the middle of the spectrum, potentially obscuring useful peaks. The reader is referred to the references cited in the main text for a discussion of this. In practice, both the States and echo–antiecho methods can be easily adapted to incorporate this shifting of axial peaks (in the former case it is creatively known as the *States–TPPI method*), so I do not consider it any further here.

desired double-absorption lineshape. Phase correction along ω_1 can now be carried out.*

Naturally, the obvious question is how the sine-modulated signal $s_{\sin}(t_1, t_2)$ can be obtained. Returning to the product operators in eq. (1.68), we see that we can obtain this if we change the mixing period to transform $P' \to Q$ instead of $P \to Q$. This can usually be done by phase shifting one or more pulses after the t_1 period by 90°.† Alternatively (in fact, more commonly), we can modify the preparation period such that it produces an operator $-P'$ which rotates into P during t_1. That way, after the t_1 evolution period we have a density operator of the form $-P' \cos(\omega_P t_1) + P \sin(\omega_P t_1)$; if we keep the mixing period the same then we will obtain the desired sine-modulated data. In contrast to before, this can be done by phase shifting one or more pulses before the t_1 period by −90°.

On the other hand, the echo–antiecho method seeks instead to measure two signals which are *phase-modulated* in t_1 (instead of *amplitude-modulated* as in the States method):

$$s_{\text{echo}}(t_1, t_2) = \frac{1}{2} \exp(-\mathrm{i}\Omega_P t_1) \exp(\mathrm{i}\Omega_Q t_2) \tag{1.75}$$

$$s_{\text{antiecho}}(t_1, t_2) = \frac{1}{2} \exp(\mathrm{i}\Omega_P t_1) \exp(\mathrm{i}\Omega_Q t_2) \tag{1.76}$$

Once recorded, these signals can be added and subtracted to obtain the cosine- and sine-modulated signals of the States method; the standard States processing can then follow. The echo and antiecho signals can be obtained through the use of pulsed field gradients during the t_1 period, though a concrete example is deferred until the next section. The factor of $1/2$ in eqs. (1.75) and (1.76) requires an explanation: this arises because the 'original' signal is cosine- or sine-modulated, which can be thought of as a sum of two opposite phase modulations, i.e. $\cos(\Omega_P t_1) = [\exp(-\mathrm{i}\Omega_P t_1) + \exp(\mathrm{i}\Omega_P t_1)]/2$. The gradients effectively select for only one sense of the phase modulation and reject the other. Although this factor of $1/2$ can be cancelled out

*This treatment of the States method stems from the original paper[22] and is consistently reproduced in textbooks, although I have personally always found the steps rather contrived. I argue instead that a more coherent formulation can be given in terms of *quaternions*, a type of *hypercomplex number*, expressed as $a + \mathrm{i}b + \mathrm{j}c + \mathrm{k}d$ where $a, b, c, d \in \mathbb{R}$, $\mathrm{i}^2 = \mathrm{j}^2 = \mathrm{k}^2 = -1$, and $\mathrm{ij} = -\mathrm{ji} = \mathrm{k}$. We can write that $s_{\cos} = \cos(\Omega_P t_1) \exp(\mathrm{j}\Omega_Q t_2)$, and that $s_{\sin} = \sin(\Omega_P t_1) \exp(\mathrm{j}\Omega_Q t_2)$; then, we can directly form a quaternionic 2D matrix $s(t_1, t_2) = s_{\cos} + \mathrm{i}s_{\sin} = \exp(\mathrm{i}\Omega_P t_1) \exp(\mathrm{j}\Omega_Q t_2)$. At this point, we can use a quaternion Fourier transform to *directly* obtain the data: $S(\omega_1, \omega_2) = (2\pi)^{-1} \iint \exp(-\mathrm{i}\omega_1 t_1) s(t_1, t_2) \exp(-\mathrm{j}\omega_2 t_2)$, and phase correction in *both* dimensions can be carried out at will and simultaneously using $\exp(\mathrm{i}\phi_{\text{corr},1}) S(\omega_1, \omega_2) \exp(\mathrm{j}\phi_{\text{corr},2})$, where the ϕ_{corr}'s represent the phase corrections in the two respective frequency dimensions. Indeed, in the representation of 2D data as used by Bruker machines, the four files `2rr`, `2ri`, `2ir`, and `2ii` essentially correspond to the four components (or *quadrants*) of a quaternionic $S(\omega_1, \omega_2)$. Of course, this is merely nice notation: none of the underlying science is changed. But the beauty of this is that we can consider the steps given in the main text to be an *implementation* of something more fundamental (the quaternionic Fourier transform), a generalisation which naturally follows from the 1D case and immediately suggests its extension to the 3D case, rather than a *prescription* which—at least to a novice—seems to have been plucked from thin air, working 'only as if by magic'. This treatment has been proposed before by Delsuc,[25] although it does not appear to have caught on much.

†Actually, if double-quantum coherence is sampled in t_1, then the phase shift used must be halved, i.e. 45°; and likewise for higher coherence orders. But we will not encounter such cases in this thesis.

when combining the echo and antiecho datasets, in that:

$$s_{\cos,\mathrm{EA}} = s_{\mathrm{echo}} + s_{\mathrm{antiecho}} = \cos(\Omega_P t_1)\exp(\mathrm{i}\Omega_Q t_2) = s_{\cos} \tag{1.77}$$

(and likewise for the sine component), the process of adding up two separate datasets leads to a $\sqrt{2}$ increase in the noise level when compared to measuring $s_{\cos}$ directly. Therefore, echo–antiecho spectra have a $\sqrt{2}$ decrease in signal-to-noise ratio (SNR) compared to their States counterparts. This point is explored more fully in an article by Keeler and coworkers.[26] Despite this loss in SNR, the use of gradients typically leads to spectra with far better artefact suppression, completely obviating the need for long phase cycles. Consequently, a significant proportion of modern 2D experiments use echo–antiecho selection.

1.4.4 The States HSQC experiment

To illustrate the ideas developed in the previous section, we now turn our attention to two typical implementations of the 2D HSQC experiment, where both phase cycling as well as gradients are used to select for particular product operators. Figure 1.6 shows an HSQC experiment where quadrature detection in the indirect dimension is performed using the States method.

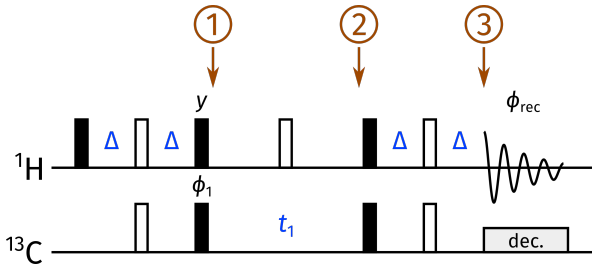

Figure 1.6: A typical HSQC pulse sequence utilising the States method for quadrature detection in ω_1. The delay Δ is set to $1/(4 \cdot {}^1J_{\mathrm{CH}})$. To record the cosine-modulated dataset $s_{\cos}(t_1, t_2)$, we set $\phi_1 = \phi_{\mathrm{rec}} = (x, -x)$. The sine-modulated dataset $s_{\sin}(t_1, t_2)$, on the other hand, is obtained using $\phi_1 = (-y, y)$ and $\phi_{\mathrm{rec}} = (x, -x)$.

The HSQC experiment seeks to only detect protons directly bonded to ^{13}C; all other protons must be suppressed. We first consider the simplest possible implementation of the HSQC, that shown in fig. 1.6; as before, we will illustrate this with an *IS* spin pair. It can be shown that the equilibrium *S*-magnetisation cannot be transformed into observable *I*-magnetisation at the end of the sequence, so we will simply take $\rho_0' = I_z$. Consider first the 'basic' case where $\phi_1 = x$. The *preparation period* is just the same INEPT element as analysed in § 1.4.2, so at point ① we already know that we have

$$\rho = -2I_z S_y. \tag{1.78}$$

During t_1 this evolves to give:

$$\rho = 2I_zS_y\cos(\Omega_S t_1) - 2I_zS_x\sin(\Omega_S t_1), \tag{1.79}$$

at point ②, bearing in mind that the $180^\circ_x(I)$ pulse inverts the I_z term. Immediately after this, the reverse INEPT element (the 'mixing' segment) transfers the amplitude-modulated $2I_zS_y$ coherence I_x for detection. However, the $2I_zS_x$ term is turned into a mixture of unobservable zero- and double-quantum coherence, such that immediately before detection (point ③) we have:

$$\rho = I_x\cos(\Omega_S t_1) = \frac{1}{2}(I_+ + I_-)\cos(\Omega_S t_1). \tag{1.80}$$

Performing the usual quadrature detection in the direct t_2 dimension gives us the desired cosine-modulated signal of

$$s_{\cos}(t_1, t_2) = \frac{1}{2}\cos(\Omega_S t_1)\exp(\mathrm{i}\Omega_I t_2), \tag{1.81}$$

In a similar way, it can be shown that setting $\phi_1 = -y$ yields the following after t_1 (point ②)

$$\rho = 2I_zS_x\cos(\Omega_S t_1) + 2I_zS_y\sin(\Omega_S t_1), \tag{1.82}$$

which after the reverse INEPT gives us the desired sine-modulated signal

$$s_{\sin}(t_1, t_2) = \frac{1}{2}\sin(\Omega_S t_1)\exp(\mathrm{i}\Omega_I t_2). \tag{1.83}$$

These can be combined in the way described in § 1.4.3 to yield an HSQC spectrum with double absorption-mode lineshapes $A_1(\Omega_S)A_2(\Omega_I)$.

This alone is not sufficient to obtain a high-quality HSQC spectrum, however. Not every ^{1}H spin in a molecule will share a one-bond coupling to a ^{13}C spin: for example, in a natural-abundance sample, the HSQC experiment only detects $\sim$ 1% of ^{1}H spins. Even small artefacts arising from the remaining $\sim$ 99% proton magnetisation may have comparable intensity to the signals of interest. We therefore need to suppress any unwanted peaks which might arise from this '*bulk*' magnetisation.

The simplest way to do this is to perform (at least) a two-step phase cycle, where the pulse phase ϕ_1 and receiver phase ϕ_{rec} are simultaneously inverted. This has no effect on the desired signal (it picks up two minus signs which cancel out), but will lead to cancellation of any signal arising from the bulk magnetisation, which does not evolve under H_J and therefore cannot be affected by the pulse on spin *S*. Note the similarity to the INEPT phase cycling in § 1.4.2, where we chose to cycle a pulse which the undesired pathway did not 'experience': this is not the only possible choice, but is conceptually simple to understand. Naturally, this phase cycling must be carried out for both the cosine- and sine-modulated datasets. In practice, even longer phase cycles are typically required to deal with experimental imperfections.

1.4.5 The echo–antiecho HSQC: gradients and coherence selection

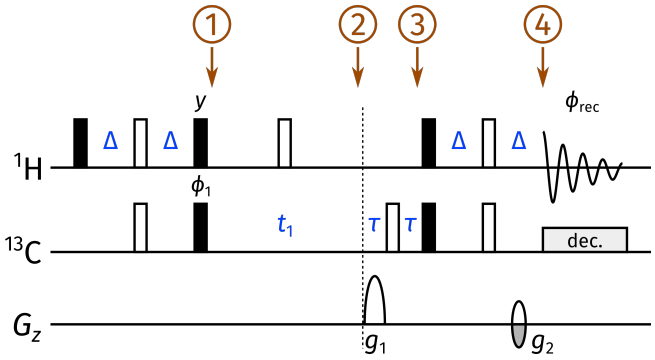

Figure 1.7: A typical echo–antiecho HSQC pulse sequence. The delay Δ is set to $1/(4{\cdot}{}^1J_{CH})$. The gradient amplitudes are chosen such that $|g_1/g_2| = \gamma_H/\gamma_C \approx 4$. Specifically, the echo dataset is obtained by setting $(g_1, g_2) = (80\%, 20\%)$, and the antiecho dataset by setting $(g_1, g_2) = (80\%, -20\%)$, where gradient amplitudes are quoted as a percentage of the maximum gradient amplitude. Unlike in the States HSQC (fig. 1.6), phase cycling of ϕ_1 and ϕ_{rec} is no longer mandatory as the gradients g_1 and g_2 dephase unwanted magnetisation. τ represents the duration of both gradients (usually on the order of 1 ms).

The echo–antiecho version of the HSQC experiment (fig. 1.7) is very similar to the States version discussed above. The only real difference is that two gradients are added: one immediately after t_1, and one directly before detection. As we will see, the effect of this is to enforce a relationship between the coherence orders during the two gradients, or in other words, to select for a specific *coherence transfer pathway* (CTP).

Recall that the Hamiltonian caused by a gradient of strength G is given by $H_{grad} = \sum_i \gamma_i G z I_{iz}$ (eq. (1.10)), where z is the z-position of the spin. In the case of our two-spin system, we can more explicitly write this as:

$$H_{grad} = \gamma_I G z I_z + \gamma_S G z S_z. \tag{1.84}$$

Points ① and ② are the same as in the States HSQC (fig. 1.6), so from eq. (1.79) we know that the density operator at point ② is:

$$\rho = 2I_z S_y \cos(\Omega_S t_1) - 2I_z S_x \sin(\Omega_S t_1). \tag{1.85}$$

In the next spin echo with the gradient g_1, H_{offset} and H_J are refocused, so we can ignore their effects. We assume here that the CTP gradients are applied with duration τ.* The I_z terms in ρ are unaffected by the gradient since they commute with H_{grad}; however, the transverse S-magnetisation is rotated by a phase which depends on the position of the spin system in the

*In practice, we also need to include a gradient recovery delay immediately after the gradient to allow for the dissipation of eddy currents, which causes the spin echo to be lengthened slightly. This is inconsequential to the analysis and will be ignored here.

sample. Immediately after the gradient, we have:

$$\begin{aligned}\rho(z) = {} & 2I_zS_y\cos(\Omega_S t_1)\cos(\gamma_S g_1 z\tau) - 2I_zS_x\cos(\Omega_S t_1)\sin(\gamma_S g_1 z\tau) \\ & - 2I_zS_x\sin(\Omega_S t_1)\cos(\gamma_S g_1 z\tau) - 2I_zS_y\sin(\Omega_S t_1)\sin(\gamma_S g_1 z\tau),\end{aligned} \tag{1.86}$$

where the $\rho(z)$ reminds us that this density matrix is spatially dependent. The $180^\circ_x(S)$ pulse then flips the S_y terms to give us, at point ③,

$$\begin{aligned}\rho(z) = {} & -2I_zS_y\cos(\Omega_S t_1)\cos(\gamma_S g_1 z\tau) - 2I_zS_x\cos(\Omega_S t_1)\sin(\gamma_S g_1 z\tau) \\ & - 2I_zS_x\sin(\Omega_S t_1)\cos(\gamma_S g_1 z\tau) + 2I_zS_y\sin(\Omega_S t_1)\sin(\gamma_S g_1 z\tau).\end{aligned} \tag{1.87}$$

We know already from the States HSQC analysis that the mixing period (i.e. reverse INEPT) causes the transformation $2I_zS_y \rightarrow I_x$, and that the $2I_zS_x$ term is lost. So, *if* the gradient g_2 were absent, we would have the following terms at point ④:

$$\begin{aligned}\rho(z) &= -I_x\cos(\Omega_S t_1)\cos(\gamma_S g_1 z\tau) + I_x\sin(\Omega_S t_1)\sin(\gamma_S g_1 z\tau) \\ &= -I_x\cos(\Omega_S t_1 + \gamma_S g_1 z\tau).\end{aligned} \tag{1.88}$$

This is of course not the case. In principle, the last Δ delay should be split up into two parts: one of duration $(\Delta - \tau)$ where only $H_{\text{free},I}$ is active, and one of duration τ where the Hamiltonian $H_{\text{free}} + H_{\text{grad}}$ operates. Thankfully, we know that H_{grad} commutes with $H_{\text{free,I}}$, so we can in fact separate the relevant propagators:

$$\begin{aligned}&\exp[-\mathrm{i}(H_{\text{free},I} + H_{\text{grad}})\tau]\exp[-\mathrm{i}H_{\text{free},I}(\Delta - \tau)] \\ &\quad = \exp(-\mathrm{i}H_{\text{grad}}\tau)\exp(-\mathrm{i}H_{\text{free},I}\tau)\exp[-\mathrm{i}H_{\text{free},I}(\Delta - \tau)] \\ &\quad = \exp(-\mathrm{i}H_{\text{grad}}\tau)\exp(-\mathrm{i}H_{\text{free},I}\Delta),\end{aligned} \tag{1.89}$$

where the first (rightmost) propagator is just the delay without a gradient, and the second (leftmost) propagator is just the gradient on its own. So, we can directly apply $\exp(-\mathrm{i}H_{\text{grad}}\tau)$ to the density operator in eq. (1.88) to get:*

$$\rho(z) = -I_x\cos(\Omega_S t_1 + \gamma_S g_1 z\tau)\cos(\gamma_I g_2 z\tau) - I_y\cos(\Omega_S t_1 + \gamma_S g_1 z\tau)\sin(\gamma_I g_2 z\tau) \tag{1.90}$$

$$\begin{aligned}= {} & -\frac{1}{2}I_x\cos[\Omega_S t_1 + (\gamma_S g_1 + \gamma_I g_2)z\tau] - \frac{1}{2}I_x\cos[\Omega_S t_1 + (\gamma_S g_1 - \gamma_I g_2)z\tau] \\ & - \frac{1}{2}I_y\sin[\Omega_S t_1 + (\gamma_S g_1 + \gamma_I g_2)z\tau] + \frac{1}{2}I_y\sin[\Omega_S t_1 + (\gamma_S g_1 - \gamma_I g_2)z\tau]\end{aligned} \tag{1.91}$$

(as a sanity check, it can be verified that this reduces to eq. (1.88) if $g_2 = 0$). The signal which we

*We have implicitly assumed here that the z-coordinate of the *IS* spin pair during the first gradient is the same as its z-coordinate during g_2, or in other words, that there is no *diffusion* or *convection* between the two gradients. In general, this is not true, and these effects will lead to a loss of signal as the rephasing by the second gradient is not perfect.

detect stems from the entire sample length, so we in fact need to perform an integration over z:

$$\rho = \frac{1}{L} \cdot \int_{-L/2}^{L/2} \rho(z)\,\mathrm{d}z, \tag{1.92}$$

where the sample length is L and $z = 0$ is assumed to be the middle of the sample.

For the *echo* experiment, we choose the ratio $g_1/g_2 = \gamma_I/\gamma_S$; this means that $\gamma_S g_1 - \gamma_I g_2 = 0$. The second and fourth terms in eq. (1.91) thus *lose* their z-dependence; when integrated over z these terms are unchanged. On the other hand, the first and third terms are attenuated by a factor proportional to $\int_{-L/2}^{L/2} \cos[(\gamma_S g_1 + \gamma_I g_2)z\tau]\,\mathrm{d}z$ (or equivalently, the sine). The integrand here can be identified as the phase caused by the evolution under the gradient pulse; we say that the gradients *dephase* coherences. (In the case of the second and fourth terms, they also *rephase* coherences.) If the gradient strengths (g_1, g_2) and/or their durations τ are sufficiently large, the integral evaluates to a small number which is effectively zero, corresponding to complete dephasing. The result is that, just before detection, we have:

$$\rho = -\frac{1}{2} I_x \cos(\Omega_S t_1) + \frac{1}{2} I_y \sin(\Omega_S t_1), \tag{1.93}$$

or, extracting the detectable I_- components,

$$\rho = -\frac{1}{4} I_- \cos(\Omega_S t_1) + \frac{\mathrm{i}}{4} I_- \sin(\Omega_S t_1) = -\frac{1}{4} I_- \exp(-\mathrm{i}\Omega_S t_1). \tag{1.94}$$

Detection of this in t_2 gives us the echo signal

$$s_{\mathrm{echo}}(t_1, t_2) = -\frac{1}{4} \exp(\mathrm{i}\Omega_S t_1) \exp(\mathrm{i}\Omega_I t_2), \tag{1.95}$$

in accordance with eq. (1.75). Note that the prefactor here is $-1/4$, instead of $1/2$ in the States method (eqs. (1.81) and (1.83)): this accounts for the decreased SNR in the echo–antiecho method as previously described (the minus sign comes from the extra $180^\circ(S)$ pulse after t_1, but is inconsequential as it can be removed by phase correction).

In a similar way, it can be shown that if we invert the sign of g_2, we have that $g_1/g_2 = -\gamma_I/\gamma_S$. Now, the second and fourth terms in eq. (1.91) are dephased, and we get the antiecho spectrum from this:

$$s_{\mathrm{antiecho}}(t_1, t_2) = -\frac{1}{4} \exp(-\mathrm{i}\Omega_S t_1) \exp(\mathrm{i}\Omega_I t_2). \tag{1.96}$$

In the above treatment, I have only used the 'rules' developed so far for Cartesian product operators to explain the effects of gradients. *This is clearly very tedious!* When gradients are involved, it proves simpler to use a different basis, specifically $\{E, I_z, I_+, I_-\}$. The coherence orders of these, and their products, are easily read off from the terms involved: for example, I_-S_- is double-quantum coherence with $p = -2$. The evolution of these terms under various

Hamiltonians is summarised by Keeler,[4] but two cases are particularly simple and important here:

1. 180°_x pulses invert I_z and interchange $I_+ \leftrightarrow I_-$;
2. An operator I_{ip}, on a spin i and with coherence order p, evolves under the Hamiltonian ωI_z for a time t to give:

$$I_{ip} \longrightarrow I_{ip} \exp(-\mathrm{i}p\omega t) \tag{1.97}$$

We have seen examples of the latter before: compare, for example, eqs. (1.53) and (1.54). Consider now how a spatially dependent phase is imparted to a coherence as it proceeds through the HSQC sequence. We assume that between the two gradients the coherence I_{ip} is transferred to I_{jq}, i.e. q-order coherence on some other spin j:

$$I_{ip} \xrightarrow{g_1} I_{ip} \exp(-\mathrm{i}p\gamma_i g_1 z\tau) \xrightarrow{mixing} I_{jq} \xrightarrow{g_2} I_{jq} \exp(-\mathrm{i}q\gamma_j g_2 z\tau) \exp(-\mathrm{i}p\gamma_i g_1 zt). \tag{1.98}$$

For the coherence to be rephased, we require that

$$p\gamma_i g_1 \tau + q\gamma_j g_2 \tau = 0, \tag{1.99}$$

and in the specific case of the HSQC, we know that spins i and j are respectively S and I, so

$$p\gamma_S g_1 + q\gamma_I g_2 = 0. \tag{1.100}$$

For the echo experiment, we choose $g_1/g_2 = \gamma_I/\gamma_S$, which means that this is satisfied if and only if $p + q = 0$. Since I_q is only detectable if $q = -1$, this means that $p = +1$: in other words, the gradient combination selects for the $I_z S_+$ term during t_1. We also note here that any signal generated from the bulk magnetisation (^{1}H not directly coupled to ^{13}C) cannot be rephased by these gradients: this would require that

$$p\gamma_I g_1 + q\gamma_I g_2 = 0 \Leftrightarrow p\gamma_I + q\gamma_S = 0, \tag{1.101}$$

which cannot be satisfied for any sensible integer values of p and q except for $p = q = 0$, which is not observable during t_2 anyway. So, the CTP gradients effectively remove all unwanted signals arising from the bulk magnetisation: the cycling of ϕ_1 and ϕ_{rec} done in the States experiment is rendered unnecessary.

Returning to our analysis, at the start of t_1 we had the operator $-2I_z S_y = \mathrm{i}(I_z S_+ - I_z S_-)$. For the echo experiment, we need only care about the first of these two terms. This evolves during t_1 (and the $180^\circ(I)$ pulse) to give

$$-\mathrm{i}I_z S_+ \exp(-\mathrm{i}\Omega_S t_1). \tag{1.102}$$

The gradient echo after t_1 transforms this to

$$-\mathrm{i}I_z S_- \exp(-\mathrm{i}\Omega_S t_1)\exp(-\mathrm{i}\gamma_S g_1 z\tau) = -\mathrm{i}I_z(S_x - \mathrm{i}S_y)\exp(-\mathrm{i}\Omega_S t_1)\exp(-\mathrm{i}\gamma_S g_1 z\tau). \tag{1.103}$$

Again, the mixing period only transforms $2I_zS_y \to I_x$, so we get

$$-\frac{1}{2}I_x \exp(-\mathrm{i}\Omega_S t_1)\exp(-\mathrm{i}\gamma_S g_1 z\tau) \tag{1.104}$$

just before applying the g_2 gradient. The I_x term can then be decomposed into $(I_+ + I_-)/2$, and we already know the end of the story: the I_- term is rephased by g_2 and then detected to yield $s_{\mathrm{echo}}(t_1, t_2)$ (eq. (1.95)). Being flexible in switching between the two bases can greatly simplify the mathematics involved, as terms which do not survive can be immediately dropped, and the simpler phase modulation $\exp(\mathrm{i}\omega t)$ can be used instead of unwieldy $\cos(\omega t)$ and $\sin(\omega t)$ terms.

To end this chapter, we generalise the refocusing requirement introduced in eq. (1.99). The treatment here is similar to that of Mitschang et al.[27] In general, during a pulse sequence we may have n gradients in total, with amplitudes $g^{(1)}, g^{(2)}, \ldots, g^{(n)}$. We assume that their durations $\tau^{(i)}$ are all the same, such that they can be factored out of the equation. We express the coherence during the i-th gradient as a product of single-spin coherences

$$M^{(i)} = \prod_j^{\text{spins}} I_j(p_j^{(i)}), \tag{1.105}$$

where $I_j(p_j^{(i)})$ represents $p_j^{(i)}$-order coherence on spin j during gradient i. The spatially dependent phase imparted by the gradient $g^{(i)}$ is the sum of the phases acquired by each individual coherence:

$$\phi^{(i)} = -z g^{(i)} \sum_j p_j^{(i)} \gamma_j \tag{1.106}$$

For rephasing of a CTP, we require that $\sum_i \phi^{(i)} = 0$, or equivalently

$$\sum_i \left(g^{(i)} \sum_j p_j^{(i)} \gamma_j \right) = 0. \tag{1.107}$$

We can now define a *weighted coherence order*[28] as

$$p^{(i)} = \sum_j p_j^{(i)} \gamma_j. \tag{1.108}$$

For example, the weighted coherence order for I_+S_- is simply $\gamma_I - \gamma_S$.* This allows the rephasing condition to be very simply expressed as a scalar product:

$$\sum_i g^{(i)} p^{(i)} = \mathbf{g} \cdot \mathbf{p} = 0. \tag{1.109}$$

$\mathbf{g} \cdot \mathbf{p}$ can be considered to be an 'extent of dephasing': ideally, gradient amplitudes $\mathbf{g}$ are chosen such that the desired CTP $\mathbf{p}$ is rephased (eq. (1.109)), and undesired CTPs $\mathbf{p}'$ are suppressed as much as possible in that $\mathbf{g} \cdot \mathbf{p}'$ is maximised.

1.5 References

(1) Ernst, R. R.; Bodenhausen, G.; Wokaun, A., *Principles of Nuclear Magnetic Resonance in One and Two Dimensions*; Clarendon Press: Oxford, U.K., 1987.

(2) Cavanagh, J.; Fairbrother, W. J.; Palmer III, A. G.; Rance, M.; Skelton, N. J., *Protein NMR Spectroscopy: Principles and Practice*, 2nd ed.; Academic Press: Burlington, Mass., 2007.

(3) Levitt, M. H., *Spin Dynamics: Basics of Nuclear Magnetic Resonance*, 2nd ed.; Wiley: Chichester, U.K., 2008.

(4) Keeler, J., *Understanding NMR Spectroscopy*, 2nd ed.; Wiley: Chichester, U.K., 2010.

(5) Hore, P. J.; Jones, J. A.; Wimperis, S., *NMR: The Toolkit, How Pulse Sequences Work*, 2nd ed.; Oxford University Press: Oxford, U.K., 2015.

(6) Sakurai, J. J.; Napolitano, J., *Modern Quantum Mechanics*; Cambridge University Press: Cambridge, U.K., 2021.

(7) Blum, K., *Density Matrix Theory and Applications*; Springer: Heidelberg, 2012.

(8) Cohen-Tannoudji, C.; Diu, B.; Laloë, F., *Quantum Mechanics*, 2nd ed.; Wiley: Weinheim, Germany, 2020.

(9) Breuer, H.-P.; Petruccione, F., *The Theory of Open Quantum Systems*; Oxford University Press: Oxford, U.K., 2002.

(10) Lidar, D. A. Lecture Notes on the Theory of Open Quantum Systems, 2019, DOI: 10.48550/arxiv.1902.00967.

(11) Chuang, I. L.; Gershenfeld, N.; Kubinec, M. G.; Leung, D. W. Bulk quantum computation with nuclear magnetic resonance: theory and experiment. *Proc. R. Soc. Lond. A* **1998**, *454*, 447–467, DOI: 10.1098/rspa.1998.0170.

*Mitschang et al. define a *composite coherence order* as $\sum_j p_j^{(i)} \gamma_j / \gamma_I$, using some nuclide I as a reference. This follows an earlier paper[28] where I is explicitly chosen to be ^{1}H, and has the advantage that if the experiment is homonuclear (i.e. all the spins j are simply I), the composite coherence order is the same as the coherence order. Here, I prefer not to tie the analysis to a particular nuclide as the choice of I will likely depend on the experiment under consideration. This different definition naturally induces a different choice of terminology.

(12) Jones, J. A. Quantum computing with NMR. *Prog. Nucl. Magn. Reson. Spectrosc.* **2011**, *59*, 91–120, DOI: 10.1016/j.pnmrs.2010.11.001.

(13) Findeisen, M.; Berger, S., *50 and More Essential NMR Experiments: A Detailed Guide*; Wiley: Weinheim, 2013.

(14) Claridge, T. D. W., *High-Resolution NMR Techniques in Organic Chemistry*, 3rd ed.; Elsevier: Amsterdam, 2016.

(15) Bloch, F. Nuclear Induction. *Phys. Rev.* **1946**, *70*, 460–474, DOI: 10.1103/physrev.70.460.

(16) Gupta, A.; Stait-Gardner, T.; Price, W. S. Is It Time to Forgo the Use of the Terms "Spin–Lattice" and "Spin–Spin" Relaxation in NMR and MRI? *J. Phys. Chem. Lett.* **2021**, *12*, 6305–6312, DOI: 10.1021/acs.jpclett.1c00945.

(17) Turner, C. J.; Hill, H. D. W. Artifacts in quadrature detection. *J. Magn. Reson.* **1986**, *66*, 410–421, DOI: 10.1016/0022-2364(86)90185-x.

(18) Sørensen, O. W.; Eich, G. W.; Levitt, M. H.; Bodenhausen, G.; Ernst, R. R. Product operator formalism for the description of NMR pulse experiments. *Prog. Nucl. Magn. Reson. Spectrosc.* **1984**, *16*, 163–192, DOI: 10.1016/0079-6565(84)80005-9.

(19) Morris, G. A.; Freeman, R. Enhancement of nuclear magnetic resonance signals by polarization transfer. *J. Am. Chem. Soc.* **1979**, *101*, 760–762, DOI: 10.1021/ja00497a058.

(20) Morris, G. A. Sensitivity enhancement in nitrogen-15 NMR: polarization transfer using the INEPT pulse sequence. *J. Am. Chem. Soc.* **1980**, *102*, 428–429, DOI: 10.1021/ja00521a097.

(21) Pines, A.; Gibby, M. G.; Waugh, J. S. Proton-Enhanced Nuclear Induction Spectroscopy. A Method for High Resolution NMR of Dilute Spins in Solids. *J. Chem. Phys.* **1972**, *56*, 1776–1777, DOI: 10.1063/1.1677439.

(22) States, D. J.; Haberkorn, R. A.; Ruben, D. J. A two-dimensional nuclear overhauser experiment with pure absorption phase in four quadrants. *J. Magn. Reson.* **1982**, *48*, 286–292, DOI: 10.1016/0022-2364(82)90279-7.

(23) Marion, D.; Wüthrich, K. Application of phase sensitive two-dimensional correlated spectroscopy (COSY) for measurements of ^{1}H–^{1}H spin-spin coupling constants in proteins. *Biochem. Biophys. Res. Commun.* **1983**, *113*, 967–974, DOI: 10.1016/0006-291x(83)91093-8.

(24) Keeler, J.; Neuhaus, D. Comparison and evaluation of methods for two-dimensional NMR spectra with absorption-mode lineshapes. *J. Magn. Reson.* **1985**, *63*, 454–472, DOI: 10.1016/0022-2364(85)90236-7.

(25) Delsuc, M. A. Spectral representation of 2D NMR spectra by hypercomplex numbers. *J. Magn. Reson.* **1988**, *77*, 119–124, DOI: 10.1016/0022-2364(88)90036-4.

(26) Kontaxis, G.; Stonehouse, J.; Laue, E. D.; Keeler, J. The Sensitivity of Experiments Which Use Gradient Pulses for Coherence-Pathway Selection. *J. Magn. Reson., Ser. A* **1994**, *111*, 70–76, DOI: 10.1006/jmra.1994.1227.

(27) Mitschang, L.; Ponstingl, H.; Grindrod, D.; Oschkinat, H. Geometrical representation of coherence transfer selection by pulsed field gradients in high-resolution nuclear magnetic resonance. *J. Chem. Phys.* **1995**, *102*, 3089–3098, DOI: 10.1063/1.468618.

(28) John, B. K.; Plant, D.; Heald, S. L.; Hurd, R. E. Efficient detection of CαH–HN correlations in proteins using gradient-enhanced ^{15}N HMQC-TOCSY. *J. Magn. Reson.* **1991**, *94*, 664–669, DOI: 10.1016/0022-2364(91)90158-p.

Chapter 2

Pure shift NMR

Pure shift NMR refers to the technique of acquiring NMR spectra free of multiplet structure, such that every chemical environment gives rise to a singlet.[1,2] In the context of this thesis, we use the term 'pure shift' exclusively to refer to broadband homodecoupled ^{1}H spectra. Here, 'broadband' means that the couplings are removed from the entire spectrum, as opposed to just a subset of it (which can be accomplished through band-selective refocusing). 'Homodecoupled' refers to the fact that the primary target here is the removal of homonuclear couplings, which cannot be done simply through decoupling during acquisition. Finally, although pure shift techniques can be applied to any nuclide, ^{1}H spectra are of greatest interest because of the narrow chemical shift range of ^{1}H which often leads to peak overlap.

In this chapter, I first cover the theory underpinning, and a brief history of, pure shift experiments. I then describe a variety of approaches aimed at increasing the quality of pure shift experiments: this is measured both in terms of *sensitivity* as well as *purity*, i.e. the lack of spectral artefacts arising from imperfect decoupling. In all cases, we compare these against the state-of-the-art PSYCHE pure shift method.[3,4] Finally, I end with a section discussing the combination of pure shift diffusion spectroscopy—formally a pseudo-3D experiment—with the use of ultrafast (single-scan) NMR techniques to collapse the diffusion dimension. This project was carried out in collaboration with Jean-Nicolas Dumez (University of Nantes).

The work in this chapter has not been submitted for publication.

2.1 Introduction

- Theory of pure shift NMR – $\{I_\alpha, I_\beta, I_+, I_-\}$ basis as explained in refs.[5–7] Include link to (absorption-mode) 2DJ spectroscopy.[8] See Pell & Keeler[9]

- Overview of (non-PSYCHE) experimental methods: BIRD, Zangger–Sterk,[10] maybe time-reversal (perhaps it can be described in more detail later)
- Real-time vs interferogram approaches. Briefly mention SAPPHIRE[11]—we can talk about it in more detail in the NOAH section.
- PSYCHE[3,4] in more detail. Spatiotemporal averaging.[12] Flip angle control. TSE version.[13] Mention ZQS[14] and GEMSTONE.[15]
- Applications of pure shift NMR: improved resolution, the TOCSY paper,[16] PSYCHE-iDOSY,[17] psNOE for distances,[18] mixture analysis, ... (what else have they come up with recently?? Probably steal some references from other people's theses...)

2.2 Direct optimisation of PSYCHE

This was stuff briefly pursued during my 2nd CDT rotation. It didn't work very well—it's just insensible to try to optimise every point in a shaped pulse, and especially not experimentally. But it did ultimately get expanded into POISE...

2.3 PSYCHE with variable number of saltire pulses

PSYCHE with 1 or 4 saltires.

There are some half-interesting results, but I don't think there was anything conclusively better than PSYCHE.

2.4 Time-reversal method

This is basically the report which we sent to Gareth Morris (and was subsequently circulated amongst lots of people...). The conclusion was that it's got sensitivity which is comparable to PSYCHE but the artefact cancellation was very poor.

2.5 'Discrete PSYCHE'

More recent work mostly involving simulations.

2.6 Ultrafast PSYCHE-iDOSY

Collaborative stuff with Jean-Nicolas Dumez which never quite went anywhere (sadly)—although at EUROMAR, JND told me he now had a student (or a postdoc?) working on it and that they might send us some stuff.

2.7 References

(1) Zangger, K. Pure shift NMR. *Prog. Nucl. Magn. Reson. Spectrosc.* **2015**, *86-87*, 1–20, DOI: 10.1016/j.pnmrs.2015.02.002.

(2) Castañar, L. Pure shift ^{1}H NMR: what is next? *Magn. Reson. Chem.* **2017**, *55*, 47–53, DOI: 10.1002/mrc.4545.

(3) Foroozandeh, M.; Adams, R. W.; Meharry, N. J.; Jeannerat, D.; Nilsson, M.; Morris, G. A. Ultrahigh-Resolution NMR Spectroscopy. *Angew. Chem., Int. Ed.* **2014**, *53*, 6990–6992, DOI: 10.1002/anie.201404111.

(4) Foroozandeh, M.; Morris, G. A.; Nilsson, M. PSYCHE Pure Shift NMR Spectroscopy. *Chem. Eur. J.* **2018**, *24*, 13988–14000, DOI: 10.1002/chem.201800524.

(5) Keeler, J., *Understanding NMR Spectroscopy*, 2nd ed.; Wiley: Chichester, U.K., 2010.

(6) Thrippleton, M. J.; Edden, R. A. E.; Keeler, J. Suppression of strong coupling artefacts in J-spectra. *J. Magn. Reson.* **2005**, *174*, 97–109, DOI: 10.1016/j.jmr.2005.01.012.

(7) Griesinger, C.; Sørensen, O. W.; Ernst, R. R. Correlation of connected transitions by two-dimensional NMR spectroscopy. *J. Chem. Phys.* **1986**, *85*, 6837–6852, DOI: 10.1063/1.451421.

(8) Aue, W. P.; Karhan, J.; Ernst, R. R. Homonuclear broad band decoupling and two-dimensional J-resolved NMR spectroscopy. *J. Chem. Phys.* **1976**, *64*, 4226–4227, DOI: 10.1063/1.431994.

(9) Pell, A. J.; Keeler, J. Two-dimensional J-spectra with absorption-mode lineshapes. *J. Magn. Reson.* **2007**, *189*, 293–299, DOI: 10.1016/j.jmr.2007.09.002.

(10) Zangger, K.; Sterk, H. Homonuclear Broadband-Decoupled NMR Spectra. *J. Magn. Reson.* **1997**, *124*, 486–489, DOI: 10.1006/jmre.1996.1063.

(11) Moutzouri, P.; Chen, Y.; Foroozandeh, M.; Kiraly, P.; Phillips, A. R.; Coombes, S. R.; Nilsson, M.; Morris, G. A. Ultraclean pure shift NMR. *Chem. Commun.* **2017**, *53*, 10188–10191, DOI: 10.1039/c7cc04423b.

(12) Dumez, J.-N. Spatial encoding and spatial selection methods in high-resolution NMR spectroscopy. *Prog. Nucl. Magn. Reson. Spectrosc.* **2018**, *109*, 101–134, DOI: 10.1016/j.pnmrs.2018.08.001.

(13) Foroozandeh, M.; Adams, R. W.; Kiraly, P.; Nilsson, M.; Morris, G. A. Measuring couplings in crowded NMR spectra: pure shift NMR with multiplet analysis. *Chem. Commun.* **2015**, *51*, 15410–15413, DOI: 10.1039/c5cc06293d.

(14) Thrippleton, M. J.; Keeler, J. Elimination of Zero-Quantum Interference in Two-Dimensional NMR Spectra. *Angew. Chem., Int. Ed.* **2003**, *42*, 3938–3941, DOI: 10.1002/anie.200351947.

(15) Kiraly, P.; Kern, N.; Plesniak, M. P.; Nilsson, M.; Procter, D. J.; Morris, G. A.; Adams, R. W. Single-Scan Selective Excitation of Individual NMR Signals in Overlapping Multiplets. *Angew. Chem., Int. Ed.* **2021**, *60*, 666–669, DOI: 10.1002/anie.202011642.

(16) Foroozandeh, M.; Adams, R. W.; Nilsson, M.; Morris, G. A. Ultrahigh-Resolution Total Correlation NMR Spectroscopy. *J. Am. Chem. Soc.* **2014**, *136*, 11867–11869, DOI: 10.1021/ja507201t.

(17) Foroozandeh, M.; Castañar, L.; Martins, L. G.; Sinnaeve, D.; Poggetto, G. D.; Tormena, C. F.; Adams, R. W.; Morris, G. A.; Nilsson, M. Ultrahigh-Resolution Diffusion-Ordered Spectroscopy. *Angew. Chem. Int. Ed.* **2016**, *55*, 15579–15582, DOI: 10.1002/anie.201609676.

(18) Kaltschnee, L.; Knoll, K.; Schmidts, V.; Adams, R. W.; Nilsson, M.; Morris, G. A.; Thiele, C. M. Extraction of distance restraints from pure shift NOE experiments. *J. Magn. Reson.* **2016**, *271*, 99–109, DOI: 10.1016/j.jmr.2016.08.007.

Chapter 3

POISE

This chapter describes the development of software for on-the-fly optimisation of NMR experimental parameters, titled POISE (*Parameter Optimisation by Iterative Spectral Evaluation*). The primary benefit of this is that parameters may be adjusted for individual spectrometers and samples, which may vary greatly in their chemical properties. POISE is primarily written in Python 3. In this chapter, I first provide some details about the implementation of POISE. The bulk of the text which follows is devoted to a number of applications in liquid-state NMR spectroscopy. At the end, the extension of the concept of on-the-fly optimisation to ESR spectroscopy is also briefly discussed: I contributed code for this, but the experimental ESR work and data analysis were carried out by Jean-Baptiste Verstraete.

The work in this chapter forms the subject of two publications:

- Yong, J. R. J.; Foroozandeh, M. On-the-Fly, Sample-Tailored Optimization of NMR Experiments. *Anal. Chem.* **2021**, *93*, 10735–10739, DOI: 10.1021/acs.analchem.1c01767
- (JBV, JY, MF, to be published)

3.1 Introduction

The paper[1]

The POISE chapter is likely to very closely follow the publication. This is the most self-contained section of my work—the only difference I want to do is to point out limitations, or cases where things didn't work as well.

Introduction should probably cover a bit more optimisation theory, e.g. Nelder–Mead. It doesn't have to be too formal but I should probably explain the differences between the algorithms.

3.2 Implementation

Behind-the-scenes look at the Python 3 implementation.

3.3 Applications

3.3.1 Pulse width calibration

`popt` vs `pulsecal`

3.3.2 Ernst angle optimisation

Maths

3.3.3 NOE mixing time

Stuff

3.3.4 ASAP-HSQC excitation delay

INEPT

3.3.5 HMBC low-pass J-filter

Artefacts.

3.3.6 Inversion–recovery

Stuff

3.3.7 Ultrafast NMR

EPSI gradient imbalance

3.3.8 PSYCHE pure shift NMR

J-refocusing

3.3.9 Solvent suppression

Mouse

3.3.10 Diffusion NMR

Automated DOSY

3.4 POISE for ESR

Need JB to write this section

3.5 References

(1) Yong, J. R. J.; Foroozandeh, M. On-the-Fly, Sample-Tailored Optimization of NMR Experiments. *Anal. Chem.* **2021**, *93*, 10735–10739, DOI: 10.1021/acs.analchem.1c01767.

Chapter 4

NOAH

This final—but long—chapter describes my work on *NOAH* (NMR by Ordered Acquisition using ^{1}H detection) *supersequences*, pulse sequences which record multiple 2D datasets in the time required for one.[1] This is an attractive NMR technique for several reasons: the time savings (which also translate into sensitivity per unit time increases) are clearly a key factor, but the flexibility of combining almost any set of 2D experiments ('modules') also makes NOAH supersequences applicable to a variety of contexts. Furthermore, the data obtained after processing is virtually identical to well-known standard 2D experiments, meaning that the results are intuitive even to non-experts in NMR.

I begin by introducing the concepts underlying NOAH supersequences, as well as a general discussion of the time savings (and sensitivity per unit time) benefits thus realised. I then describe the GENESIS (GENEration of Supersequences In Silico) website, which allows users to trivially generate NOAH supersequences containing arbitrary modules. After this, my work on various aspects of NOAH supersequences is described, with a special focus on newly developed and/or improved modules. Finally, the design of 'parallel' supersequences which use interleaved and/or time-shared modules is discussed.

This work was done in close collaboration with Ēriks Kupče (Bruker UK). However, all results and analysis shown in this thesis are mine, unless explicitly stated. The work in this chapter forms the subject of several publications:

- Yong, J. R. J.; Hansen, A. L.; Kupče, Ē.; Claridge, T. D. W. Increasing sensitivity and versatility in NMR supersequences with new HSQC-based modules. *J. Magn. Reson.* **2021**, *329*, 107027, DOI: 10.1016/j.jmr.2021.107027
- Kupče, Ē.; Yong, J. R. J.; Widmalm, G.; Claridge, T. D. W. Parallel NMR Supersequences: Ten Spectra in a Single Measurement. *JACS Au* **2021**, *1*, 1892–1897, DOI: 10.1021/jacsa

u.1c00423

- Yong, J. R. J.; Kupče, Ē.; Claridge, T. D. W. Modular Pulse Program Generation for NMR Supersequences. *Anal. Chem.* **2022**, *94*, 2271–2278, DOI: 10.1021/acs.analchem.1c04964
- ABBS paper to be submitted

The material in the introductory sections also closely follow two reviews which I have contributed to:

- Kupče, Ē.; Frydman, L.; Webb, A. G.; Yong, J. R. J.; Claridge, T. D. W. Parallel nuclear magnetic resonance spectroscopy. *Nat. Rev. Methods Primers* **2021**, *1*, No. 27, DOI: 10.1038/s43586-021-00024-3
- RSC book chapter

4.1 Introduction

The opening sections for the NOAH chapter will likely be very similar to the recent RSC book chapter. That was written quite recently so reflects my current perspective quite accurately, and I am quite happy with the way it was laid out (in contrast to the *Nature Reviews Methods Primers* work).

Magnetisation pools, etc.

4.2 Sensitivity analysis of NOAH supersequences

General discussion of time savings and sensitivity analysis.

Should be very similar to RSC chapter

4.3 GENESIS: automated pulse programme creation

I think it makes sense to start with GENESIS;[4] that way everything else can be placed in context.

It's true that this was a full paper, but it included a lot of stuff which wasn't about the website itself—these will go into later sections.

4.4 Discussion of individual modules

4.4.1 Sensitivity-enhanced HSQC

^{13}C seHSQC

^{15}N seHSQC

4.4.2 HSQC-TOCSY

HSQC + DIPSI + HSQC combos

Extension to HSQC-TOCSY

Cite ASAP work (Luy)

4.4.3 HSQC-COSY

Comparison of several versions of HSQC-COSY (JACS Au SI)

4.4.4 2DJ and PSYCHE

cnst37 scaling

SAPPHIRE

4.4.5 DQF-COSY

Once upon a time, I did some comparisons of States vs EA DQF-COSY. I think this section could probably be left out, though. The differences were *extremely* minor.

4.4.6 HMQC

Suppression of wing artefacts (GENESIS paper)

4.4.7 HMBC

Suppression of $^{1}J_{\mathrm{CH}}$ artefacts (GENESIS paper)

Investigation of gradient schemes (no difference was really observed, but that's fine)

Also ^{15}N HMBC

4.4.8 ADEQUATE

Recent stuff.

4.5 Solvent suppression in NOAH

GENESIS paper.

4.6 NOAH with short relaxation delays (???)

I did like one bit of work on this a while ago. The idea is basically that the spectra are fine but SNR unsurprisingly suffers (in fact SNR/t also decreases).

It may be mildly interesting to compare this against the NORD experiments if I can get their pulse programmes to work... I don't expect the NORD sensitivity to be amazing but it should in fact be better than just doing NOAH with short d1.

It may equally be viable to just leave this entire section out of the thesis as I don't think it adds much...

4.7 Parallel and generalised NOAH supersequences

Blah.

4.8 References

(1) Kupče, Ē.; Claridge, T. D. W. NOAH: NMR Supersequences for Small Molecule Analysis and Structure Elucidation. *Angew. Chem. Int. Ed.* **2017**, *56*, 11779–11783, DOI: 10.1002/anie.201705506.

(2) Yong, J. R. J.; Hansen, A. L.; Kupče, Ē.; Claridge, T. D. W. Increasing sensitivity and versatility in NMR supersequences with new HSQC-based modules. *J. Magn. Reson.* **2021**, *329*, 107027, DOI: 10.1016/j.jmr.2021.107027.

(3) Kupče, Ē.; Yong, J. R. J.; Widmalm, G.; Claridge, T. D. W. Parallel NMR Supersequences: Ten Spectra in a Single Measurement. *JACS Au* **2021**, *1*, 1892–1897, DOI: 10.1021/jacsau.1c00423.

(4) Yong, J. R. J.; Kupče, Ē.; Claridge, T. D. W. Modular Pulse Program Generation for NMR Supersequences. *Anal. Chem.* **2022**, *94*, 2271–2278, DOI: 10.1021/acs.analchem.1c04964.

(5) Kupče, Ē.; Frydman, L.; Webb, A. G.; Yong, J. R. J.; Claridge, T. D. W. Parallel nuclear magnetic resonance spectroscopy. *Nat. Rev. Methods Primers* **2021**, *1*, No. 27, DOI: 10.1038/s43586-021-00024-3.

List of figures

List of tables

Appendix A

Other work

I'm not sure I'll actually get to this, but I think it would be nice to write something about these, because a fair bit of 'work' has gone into these.

My other big(-ish) software projects were of course part of the thesis.

Project	File extensions included	Total lines of code
`nmrpoise`	`.py`, `.rst`, `.sh`	6047
`genesis`	`.js`, `.ts`, `.html`, `.css`, `.sh`	11330[a]
`matlab_nmr_jy`	`.m`, `.py`	7961[b]
`penguins`	`.py`, `.rst`	7129
`abbotsbury`	`.hs`	5446
`nmrespy`[1]	`.py`, `.rst`	19007
`spinach-2.6.5625`[2]	`.m`	116443
`numpy`[3]	`.py`, `.cpp`, `.c`, `.h`, `.f`, `.rst`	685300

Table A.1: Lines of source code in some of my software projects (plus a handful of others for comparison), as measured on 5th August 2022 on the `master` or `main` branches. Note that number of lines is a **very** poor metric for project size or complexity.

[a] Note that this includes *a lot* of raw pulse programme text, which probably inflates this number quite a bit. To 'compensate' for this, I didn't include any of the TopSpin processing scripts in the count.

[b] This includes some 800 lines of `fminlbfgs.m` which was taken from the Internet, although I did comb through it to correct some errors.

A.1 NMR plotting in Python

https://github.com/yongrenjie/penguins

A.2 Citation management

https://github.com/yongrenjie/abbotsbury

A.3 Group website and pulse programming tutorials

https://foroozandehgroup.github.io

A.4 References

(1) Hulse, S. G.; Foroozandeh, M. Newton meets Ockham: Parameter estimation and model selection of NMR data with NMR-EsPy. *J. Magn. Reson.* **2022**, *338*, 107173, DOI: 10.1016/j.jmr.2022.107173.

(2) Hogben, H. J.; Krzystyniak, M.; Charnock, G. T. P.; Hore, P. J.; Kuprov, I. Spinach – A software library for simulation of spin dynamics in large spin systems. *J. Magn. Reson.* **2011**, *208*, 179–194, DOI: 10.1016/j.jmr.2010.11.008.

(3) Harris, C. R. et al. Array programming with NumPy. *Nature* **2020**, *585*, 357–362, DOI: 10.1038/s41586-020-2649-2.